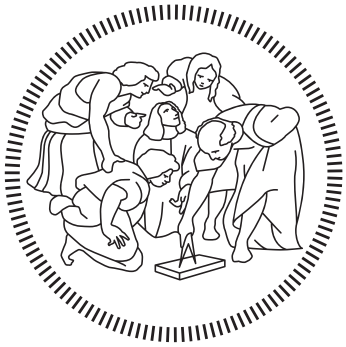

POLITECNICO
MILANO 1863

Seat Stiffness and Cushion Influence on Lumbar Spine Load in Crash Landing Conditions

Tesi di Laurea Magistrale in
Aeronautical Engineering - Ingegneria Aeronautica

Author: **Marco Ferrari**

Student ID: 232468
Advisor: Prof. Paolo Carlo Astori
Academic Year: 2024-25

Greetings

An endless thank you to my family, my compass, my structure, and my wings in every moment of my life. It is a privilege to live surrounded by such love and wisdom; who I am, I owe to you. Thank you to my friends, whether co-pilots, crew, or passengers, but always on board with me, now and forever. The journey would have no meaning without you. Thank you to all the staff at LaST, and especially to Professor Astori, essential engines for this final approach. Thank you, in general, to everyone who taught me something, to be rudder, elevators, and ailerons, and for giving me the tools to choose my own route. I look forward to discovering where it will lead me. And a small thank you to myself, the pilot (or maybe engineer) of this aircraft. An exceptional aircraft, for which I will always be grateful.

To my grandfather Roberto

Abstract

Many aircraft components can influence lumbar spine load during a crash landing, and each parameter must be evaluated on its own before assessing their combined effects.

This study first examines how seat stiffness affects lumbar load. A cushion, already well studied in previous investigations as a stand-alone element, is subsequently introduced to explore how the two variables together modify the results.

Dynamic sled tests compliant with EASA CS-25.561 and CS-25.562 were performed, measuring lumbar load on a dummy seated in a 50 kg rigid seat with a cushion. Each test used a different stiffness produced by installing various spring sets beneath the seat.

Compared to previous studies, where seat stiffness alone was shown to significantly influence lumbar load, specifically, with lower stiffness leading to increased lumbar forces, this study reveals a different behavior when seat cushions are introduced. The presence of a cushion decouples the dynamic interaction between the dummy and the springs. Results showed that the presence of the cushion led to an increase in lumbar load, reaching approximately 6100 N, compared to the fully rigid seat configuration, which resulted in values around 4000 N. No significant trend was observed when varying seat stiffness in the cushioned configuration, with lumbar loads consistently remaining near 6100 N. This is because the cushion overshadows the influence of seat stiffness, as the initial response is mainly governed by the seat itself, while the dummy's reaction is delayed due to the cushion's deformability.

A multibody numerical model was then created to replicate these tests and allow rapid parametric studies. After validation, the model was rescaled to a 10 kg seat, representative of typical aircraft seating, and the new numerical behavior was analyzed.

Keywords: Crashworthiness; Crash landing; CS-25 regulation; Lumbar load injury criteria; Seat; Dummy; Spring; Cushion; Experimental test; Multibody analysis; Validation method.

Abstract in lingua italiana

Molti componenti aeronautici possono influenzare il carico lombare durante un atterraggio d'emergenza e ciascun parametro deve essere valutato singolarmente prima di esaminarne gli effetti combinati.

Questo studio analizza innanzitutto come la rigidezza del sedile incida sul carico lombare. Successivamente viene introdotto un cuscino, già ampiamente studiato in precedenti indagini come elemento autonomo, per valutare come le due variabili combinate, modifichino i risultati.

Sono state eseguite prove dinamiche su slitta conformi alla normativa EASA CS-25.561 e CS-25.562, misurando il carico lombare su un manichino seduto in un sedile rigido da 50 kg con un cuscino. Ogni prova ha impiegato una rigidezza diversa ottenuta installando sotto il sedile vari set di molle.

Rispetto a studi precedenti, in cui la sola rigidezza del sedile si è dimostrata influenzare in modo significativo il carico lombare, in particolare, con un aumento del carico al diminuire della rigidezza, questo studio evidenzia un comportamento differente quando viene introdotto un cuscino. La presenza del cuscino disaccoppia infatti l'interazione dinamica tra il manichino e le molle. I risultati mostrano che l'aggiunta del cuscino porta a un incremento del carico lombare, che raggiunge circa 6100 N, rispetto alla configurazione con sedile completamente rigido, dove i valori si attestano intorno a 4000 N. Non è stata osservata alcuna tendenza significativa al variare della rigidezza del sedile in presenza del cuscino, con i carichi lombari che rimangono costanti attorno a 6100 N. Questo accade perché il cuscino domina la risposta del sistema, oscurando l'influenza della rigidezza strutturale del sedile, in quanto la risposta iniziale è principalmente governata dal sedile stesso, mentre la reazione del manichino è ritardata a causa della deformabilità del cuscino.

È stato quindi sviluppato un modello numerico multicorpo per replicare queste prove e consentire rapide analisi parametriche. Dopo la validazione, il modello è stato riscalato a un sedile da 10 kg, rappresentativo dei sedili aeronautici, e il nuovo comportamento numerico è stato analizzato.

Parole chiave: Sicurezza passiva; Atterraggio di emergenza; Normativa CS-25; Criteri di danno per carico lombare; Sedile; Manichino antropomorfo; Molla; Cuscino; Test sperimentali; Analisi multibody; Metodo di validazione.

Contents

1 | Introduction

1.1. Context and Motivations for Work

Over the years, air transport safety has seen remarkable progress, with improvements covering all aspects of the system, from aircraft design and on-board technologies to airport management, regulatory frameworks and operational procedures. As a result, air travel has become one of the safest modes of transportation available. This is supported by data from *Transport Statistics Great Britain* (TSGB) [1], which, based on data collected from 2006 to 2023, ranks air transport as the safest in terms of passenger casualty rates per billion passenger kilometers. These public data refer exclusively to accidents occurring within the UK territory; however, it is well known that in other parts of the world, the situation regarding transport safety is significantly less favorable.

Transport mode	**2023**		**Average**	
	Killed	**KSI**	**Killed**	**KSI**
Air	0.000	0.003	0.013	0.022
Rail	0.116	19.869	0.204	21.812
Water	0.695	61.817	0.500	47.314
Car	1.086	17.480	1.152	17.813
Pedal cycle	14.965	693.000	17.116	727.108
Pedestrian	16.869	269.588	19.416	304.463
Motorcycle	63.579	1169.826	71.400	1346.722

Table 1.1: Passenger Casualty Rates per Billion Passenger-Kilometres by Mode

Such remarkable results are the outcome of decades of research in both the active and passive safety domains. Active safety encompasses all measures designed to prevent accidents, while passive safety focuses on solutions aimed at reducing the severity of injuries

sustained by occupants once an impact occurs.

Aviation has historically dedicated much more effort to accident prevention. This is primarily due to the fact that when an aircraft accident occurs, it tends to result in a higher risk of injuries and fatalities compared to other modes of transport. However, it remains impossible to completely eliminate the risk of crashes, as multiple factors can contribute to creating the conditions for a risk scenario. A malfunction, a maintenance error, an external factor, or, more often, human error, can trigger a chain of events capable of bypassing accident prevention barriers.

The annual analysis of commercial aviation accidents by Airbus [2] provides a comprehensive overview of trends recorded since 1959. From Figure 1.1, it is evident that the risk of fatalities has been significantly reduced, even when compared to the enormous increase in the number of flights performed each year.

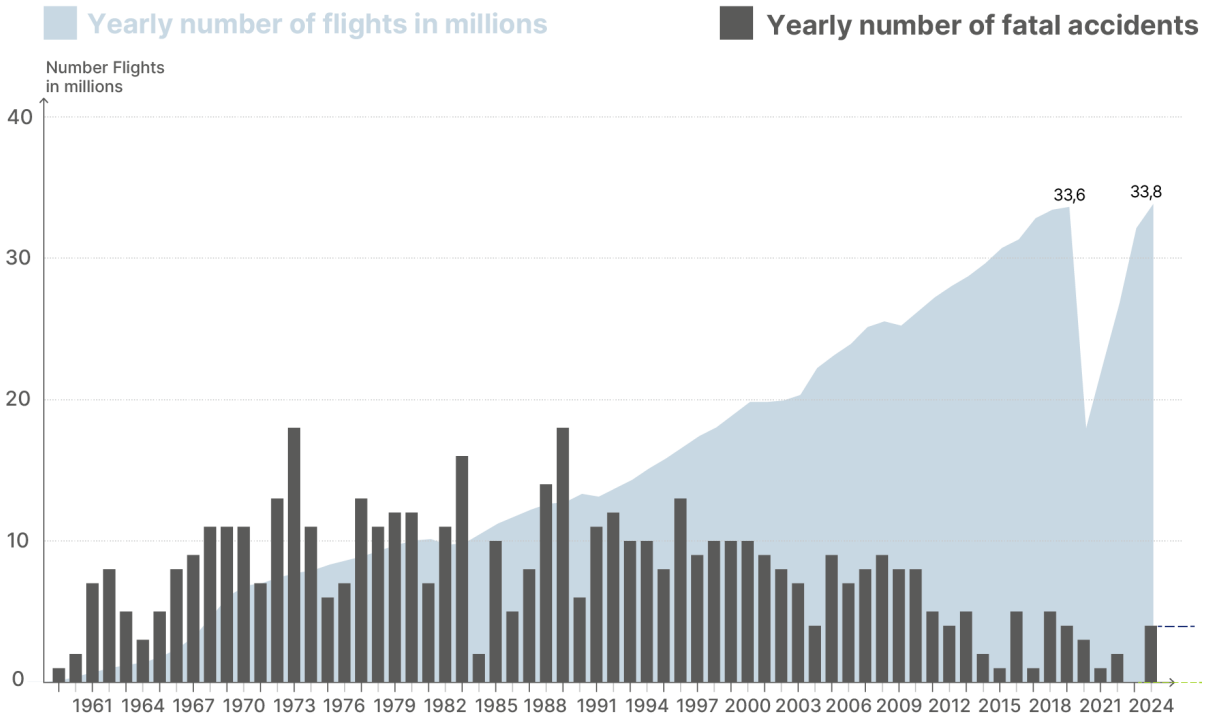

Figure 1.1: Yearly Number of Fatal Accidents 1959-2024

Furthermore, analysis of Figure 1.2 highlights the main flight phases during which incidents occur. Approach and landing are particularly complex phases, placing significant demands on the crew in terms of aircraft configuration changes (aviate), maintaining route and position control (navigate), and communication with Air Traffic Control (communicate). In addition, several other factors can increase the difficulty of the situation,

from congested airspace and degraded weather conditions to, in the worst case, technical issues. All of this occurs in scenarios that offer limited room for maneuver and little time for decision-making. This combination of high workload and the increased potential for unanticipated events can create a complex interplay of contributing factors which may lead to an accident.

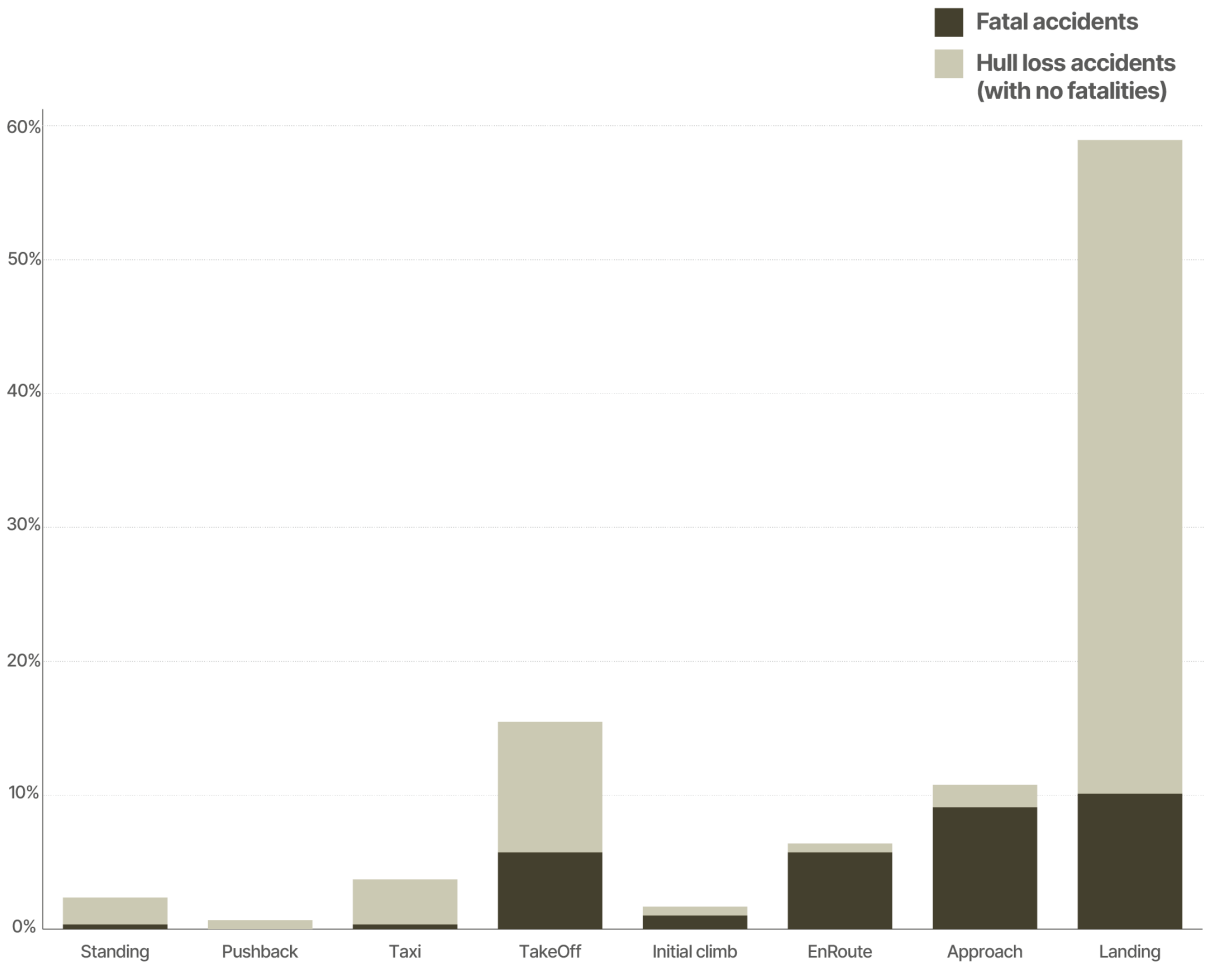

Figure 1.2: Accident Distribution per Flight Phase 2002-2024

It is also evident from Figure 1.3 that over 50% of incidents are classified under the categories of *Loss Of Control In-Flight (LOC-I)* and *Controlled Flight Into Terrain (CFIT)*, which almost certainly result in a ground (or water) impact. Other incident categories, such as *Runway Excursion (RE)*, *Undershoot/Overshoot (USOS)*, or *Fire (F-NI and F-POST)*, account for a smaller percentage. For this reason, passive safety becomes crucial, as it aims to protect occupants during impact.

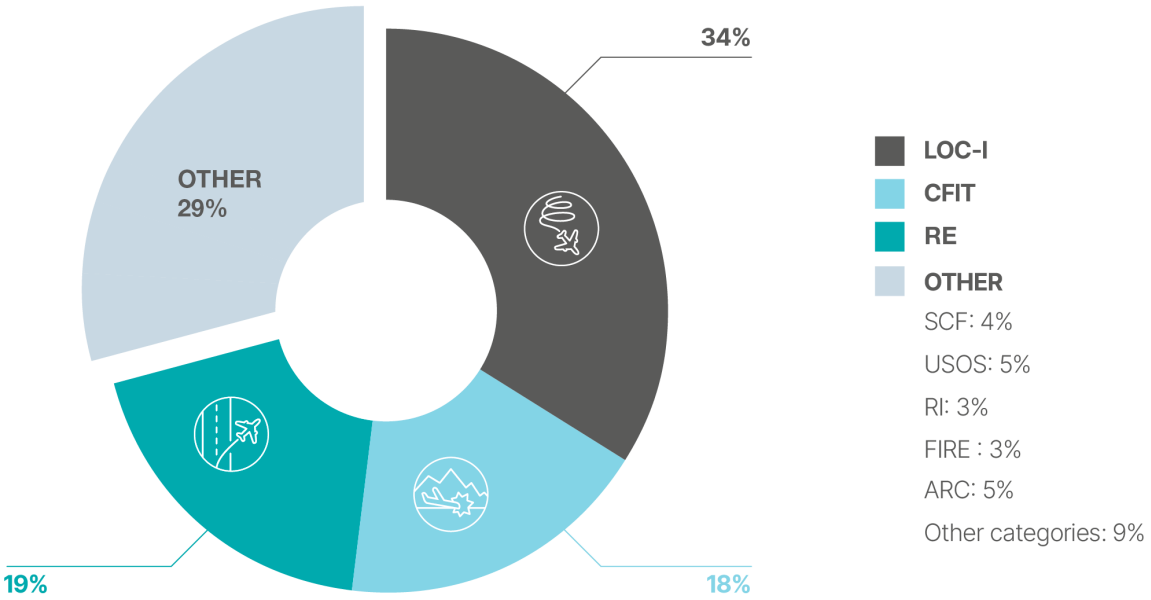

Figure 1.3: Fatal Accident Distribution per Accident Category 2004-2024

In a crash scenario, most of the energy is absorbed by the aircraft structure. Nevertheless, the impact of the fuselage with the ground (or water) transmits a considerable acceleration pulse to the cabin floor and seats, which in turn transfers it to the passenger. Therefore, in addition to other key factors, such as the strength of the airframe and the containment of flammable liquids (fuel) to prevent fire outbreaks on board, increasing attention is being given to the design and structure of passenger seats. Studies on this issue are naturally also aimed at maximizing passenger comfort during flight. However, the primary and most important challenge for seat designers is to increase the chances of survival for passengers in crash scenarios. In crash landing conditions, the seat must remain in place and absorb as much energy as possible during impact without breaking apart.

This document will explore the influence of the stiffness of an aircraft seat and the effects of the cushion on the passenger's lumbar spine in crash landing conditions. The research has been developed through both experimental tests and a numerical model.

1.2. Organization of the Work

The thesis continues in Chapter 2 with a literature review of the state of the art and the definition of the thesis objectives. Chapter 3 describes the experimental setup and the tests conducted. Chapter 4 presents and analyses the results obtained from the experimental activity, while Chapter 5 briefly introduces the multibody approach, highlighting

its advantages, and then describes the development of the numerical model using Siemens MADYMO software. Chapter 6 compares the experimental and numerical results to validate the model and analyze the outcomes. A modification to the model will be explained in Chapter 7. Finally, the main findings are summarized in Chapter 8, which also includes concluding remarks and an outlook on future developments.

2 | Literature and Thesis Aim

As previously mentioned, the seat is a fundamental component of the aircraft, as it is the part in direct contact with the occupant and ultimately the last element responsible for transmitting loads to the passenger in the event of a crash.

To gain a better understanding of the broader category of aircraft seating, the *Global Aircraft Seat Material Market (2013–2022)* [3] report by INDUSTRY ARC was analyzed. There are many different types of seats and materials used in their manufacturing, as airlines and aircraft manufacturers can select certified seat models based on their specific needs and budget constraints. For instance, seats vary depending on the type of aircraft they are installed in, such as military aircraft, long-haul aircraft, short-haul aircraft, or general aviation aircraft, as well as the travel class they are intended for, such as suite class, first class, business class, premium economy, or economy class.

Different materials are employed in seat construction to ensure they are lightweight, structurally strong, and fire-resistant. An aircraft seat typically consists of five main components: the structural frame, which is usually made of aluminum or, in some cases, carbon fiber composites; foam cushions; fire-resistant (FR) textiles; upholstery; and plastic moldings. Each airline selects specific material combinations based on factors such as cost, durability, and weight.

The global aircraft seat material market is also subject to strict regulations, with standards set by authorities such as the FAA, CASA, SAE, and EASA. These standards govern various characteristics including flame retardancy, density, and gravity performance. Seats undergo numerous qualification tests including static and dynamic load testing, vibration simulations, fatigue resistance, and overall reliability assessments.

In such a highly regulated context, it becomes crucial to understand the safety requirements that aircraft seats must meet in order to be deemed suitable for use.

2.1. Injury Criteria

First and foremost, as an integral part of the aircraft structure, the seat must fulfill the fundamental requirements of passive safety:

- Preserve the living space around the occupant.
- Prevent fire.
- Limit the accelerations transmitted to the occupant.
- Limit the impact velocities against hard surfaces.

In general, all these objectives are achieved through various engineering solutions. On one hand, a rigid survival cell is designed to preserve the occupant's living space and prevent intrusion of external objects that could cause injuries. On the other hand, deformable components are strategically integrated to absorb energy and convert it mainly into controlled plastic deformation.

This approach aims to reduce the loads and accelerations transferred to the occupant, ensuring that they do not result in severe or fatal injuries.

In fact, in a crash landing scenario, the human body is subjected to severe shocks that may lead to fractures, serious injuries (KSI), or even fatalities. For this reason, the *Certification Specifications and Acceptable Means of Compliance for Large Aeroplanes (CS-25)* [4] outlines all the safety requirements that must be met.

These include specifications regarding seat belts, which must remain securely fastened and not exceed a specified tension load for each individual strap. The seat must remain firmly attached at all anchorage points and must not yield in a way that would impede the rapid evacuation of the aircraft occupants.

Additionally, the regulation defines the so-called Injury Criteria, which establish a relationship between measured accelerations, loads, and deformations to real human body injuries. These injury criteria are indicators used to assess the severity of an impact based on measurements obtained from experimental tests on anthropomorphic test devices. They can also be scaled according to gender and age to better represent the population. In the case of a crash landing, and in line with CS-25 regulations [4], these criteria address the body regions most vulnerable during a crash landing: the head, femur, and lumbar spine. Severe trauma to any of these areas can result in paralysis, loss of consciousness, or more generally, the inability to evacuate the aircraft.

For the head, one of the most widely used criteria for assessing injury risk (specifically

brain damage or skull fracture) is the Head Injury Criterion (HIC), which is calculated as follows:

$$\mathrm{HIC} = \max\left\{(t_2 - t_1) \cdot \left[\frac{1}{t_2 - t_1}\int_{t_1}^{t_2} a(t)\,dt\right]^{2.5}\right\} \tag{2.1}$$

where $a(t)$ is the resultant acceleration of the head's center of gravity (in g's), and t_1 and t_2 represent the time interval (in seconds).

Regarding the femur, although its fracture is not in itself a fatal injury, it critically impairs mobility. A fractured femur would prevent a passenger from exiting the aircraft. To prevent this, the compressive force on the femur is limited to a maximum of $10000\,N$.

Finally, the lumbar spine is particularly vulnerable during a crash landing due to the significant vertical velocity component that typically characterizes such impacts. The resulting inertial forces can cause excessive loading on the upper body, potentially leading to an overload of the lumbar region. This overload can result in vertebral fractures and permanent damage to the spinal cord. Although not always fatal, such an injury can cause paralysis of the lower limbs, resulting in severe and lasting disability. Moreover, this type of injury poses a significant obstacle to rapid evacuation, which is critical in crash scenarios. To prevent such injuries, studies have determined that the maximum compressive load on the lumbar spine for an adult should not exceed $6670\,N$.

2.2. Regulations

In response to these survivability requirements, specific regulations have been established for the testing and certification of aircraft seats. These directives are defined in the CS-25 [4] and in the relevant *Advisory Circulars by Federal Aviation Administration (FAA)* [5], which provide practical guidance and more detailed information regarding the tests required to demonstrate compliance with the aforementioned regulations.

These documents outline the design constraints and specify the procedures needed to verify them.

In particular, the test relevant to this thesis is a single row seat evaluation, which assesses the system's performance under conditions where the primary impact force acts along the occupant's spinal column, combined with a forward-directed component. This test is intended to verify the structural integrity of the seat, the critical loads on the pelvic and lumbar regions, and any permanent deformation of the structure resulting from the

combined vertical and forward impact. Additionally, the test may provide data regarding the ATD's head displacement, velocity, and acceleration time histories.

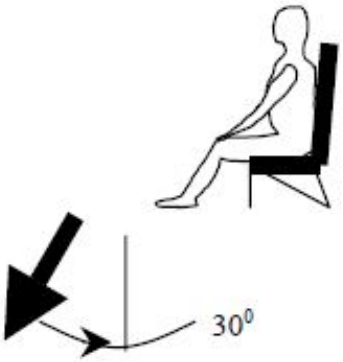

Figure 2.1: Downward Dynamic Test

The ideal acceleration pulse, which should form an angle of 30° as shown in Figure 2.1, is a triangular waveform that rises from zero to 14 g within 0.08 seconds and then returns to zero over the same time period. However, generating such an ideal pulse in a physical test is virtually impossible. Therefore, the regulations specify that the measured acceleration during testing must remain within certain defined limits.

A graphical method, provided in [5], is used to evaluate the acceleration pulse by considering its peak magnitude, duration, shape, and fluctuation over 133% of the rise time, that is the time required for the acceleration to reach its peak value. This method allows for the evaluation of whether the experimental pulse meets the required criteria, and therefore whether the data obtained from the test can be considered reliable and consistent.

The specific requirements for the acceleration and velocity profiles are as follows:

- The initial velocity must be greater than or equal to 10.70 m/s.
- The peak acceleration must be at least 14 g.
- The pulse rise time must not exceed 80 ms.
- The velocity at the end of the rise phase must be at least 5.35 m/s.
- The acceleration must always remain above the prescribed lower threshold.

To determine the rise time, a defined procedure is followed: the maximum acceleration peak is identified, and then the two points corresponding to 10% and 90% of that peak are determined. A straight line is drawn between these two points, and this line intersects the 0 g and 14 g lines at two times, identifying T_1 and T_2. The actual rise time is then

calculated based on this time interval, that is, between the intersections of this vertical line with the 0 g and 14 g levels.

At this point, T_1 is considered the start time. It is then possible to trace the ideal pulse according to the regulatory guidelines, with a peak of 14 g and an isosceles triangular waveform with a rise time of 0.08 s. At the peak, T_3 is identified, which must be greater than T_2 in order to satisfy the requirements.

Next, the velocity requirements must be verified. The velocity at the start of the pulse must be greater than 10.70 m/s. Additionally, the second velocity requirement states that, for the acquired pulse to be acceptable, V_{ra} must be at least one-half of the total velocity V, required for the specified test condition. Specifically, V_{ra} is the velocity measured up to T_3, while V is the velocity calculated up to $T_1 + 2.3 \cdot T_3$.

Finally, the shape of the sled pulse acceleration must be verified. A lower limit is constructed by drawing a triangular pulse parallel to the ideal pulse, offset by 2 g. The experimental pulse must never fall below this lower limit for the acceleration to be considered correct within the time interval $T_1 < t < T_1 + 1.33 \cdot (T_3 - T_1)$.

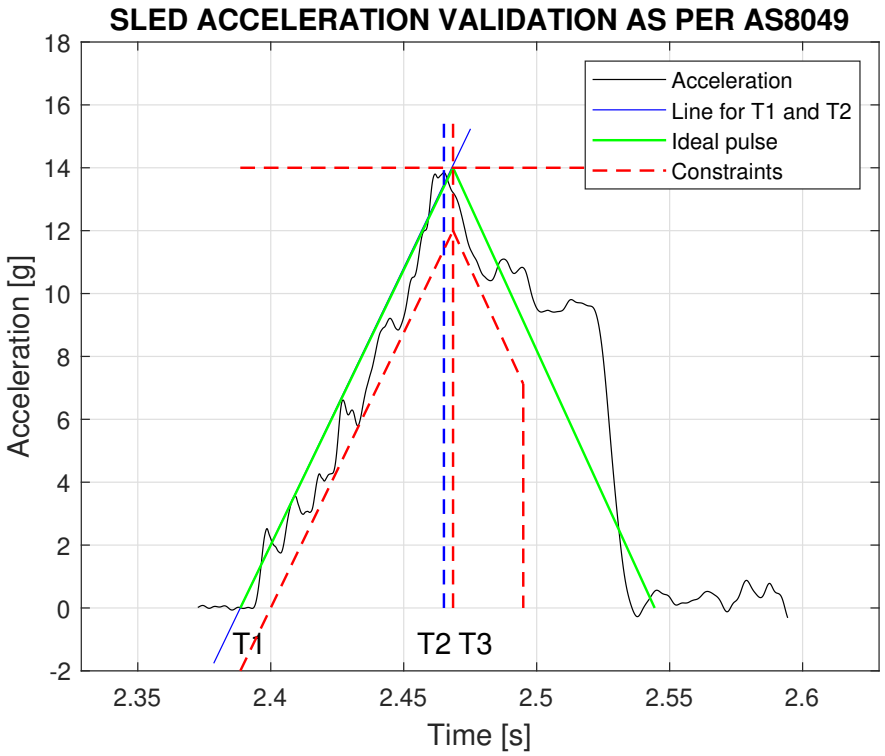

Figure 2.2: Deceleration Pulse Validation

2.3. Previous Studies

As previously mentioned, safety is a fundamental aspect in the aerospace field. It stands alongside the constant pursuit of optimization aimed at reducing fuel consumption and operational costs, working at the limit and promoting innovation and research. Ideally, increasing structural weight, by designing stronger structures, would improve passive safety. However, this approach conflicts with performance optimization, as a higher structural weight directly impacts the payload capacity.

Therefore, it is essential to find a trade-off that complies with the strict regulations imposed by civil aviation authorities. Aircraft seats are no exception. In Sections 2.1 2.2, the relevant standards and testing procedures have been presented in the context of this thesis. Research on seating systems focuses on developing lightweight structures capable of meeting stringent certification requirements.

To better understand the evolution of this field, a review of previous studies addressing these topics has been carried out.

One of the earliest and most influential contributions to the field of aviation crashworthiness and occupant survivability dates back to the 1920s, with the pioneering research of Hugh DeHaven [6]. Often referred to as the "father of aviation crashworthiness", DeHaven became interested in impact survival after surviving a mid-air collision in 1917 during pilot training with the Canadian Royal Flying Corps. He was the sole survivor, despite suffering severe internal injuries and multiple fractures. Following a lengthy recovery, DeHaven dedicated himself to investigating the causes of injuries in traumatic events such as crashes and falls. His work attracted the support of the National Research Council and the Office of Naval Research, which led to the foundation of the Crash Injury Research (CIR) program at Cornell University Medical College. In 1950, this initiative evolved into the Aviation Crash Injury Research (AvCIR) program.

Another fundamental push in the field of crashworthiness in the aeronautical sector came after the Korean and Vietnam wars. A huge number of accidents and fatalities were recorded involving helicopters. Due to their characteristics and typical operational use, especially in battlefield environments, rotorcraft impacts occurred much more frequently than those involving other types of aircraft. On behalf of the U.S. Army, these accidents were thoroughly investigated, and crashworthiness methods were developed in order to reduce fatalities and injuries. These studies led to the development of one of the most important works in the field of aircraft crashworthiness: the *Aircraft Crash Survival Design Guide*. First published in 1980 and later revised in 1989, this guide is divided into five

volumes, each focused on analyzing and proposing solutions for crashworthy design in aviation.

For example, Volume II [7] explores crash impact conditions and human tolerance to global accelerations, starting from the Eiband curves, an old but still widely used and useful reference. Derived from Col. Stapp's sled test data, these analyses form the basis for the definition of injury criteria. Volume I [8], on the other hand, presents design criteria and checklists meant to help engineers during the crashworthy design phase. Volumes III and IV [9] [10] address aircraft structural crash resistance, as well as the design of seats, restraint systems, stretchers, and cockpit/cabin delethalization strategies.

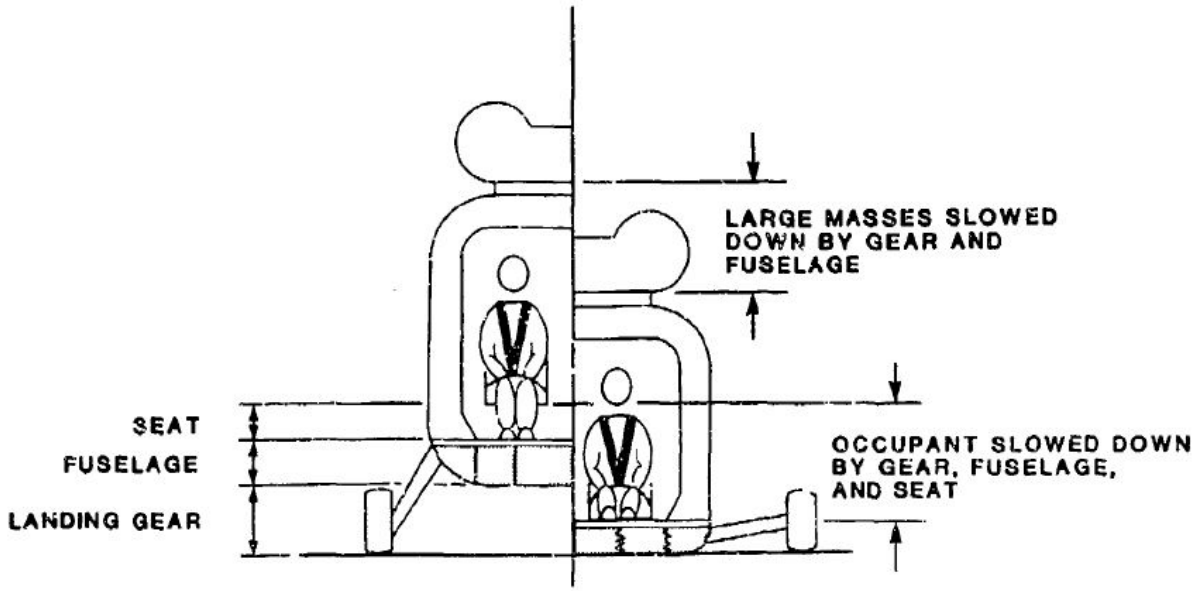

Figure 2.3: Energy Management System

Figure 2.3, taken from [9], illustrates the main structural elements designed to absorb energy in the event of a rotorcraft crash. Three primary stages of energy absorption can be identified before the load is transferred to the occupant: the landing gear, the subfloor, and the seat. This sequence is particularly relevant for helicopters and is also especially applicable to general aviation. In this sector, the number of ground impact events is significantly higher compared to commercial aviation. Nevertheless, even commercial aircraft are designed following similar crashworthiness principles and methodologies.

Therefore, under crash landing conditions, the first component involved is the landing gear, followed by the subfloor and the fuselage, and finally the seat, which transmits the load to the occupant, thus acting as the last passive barrier. Hence, it is relevant to study the seat in detail.

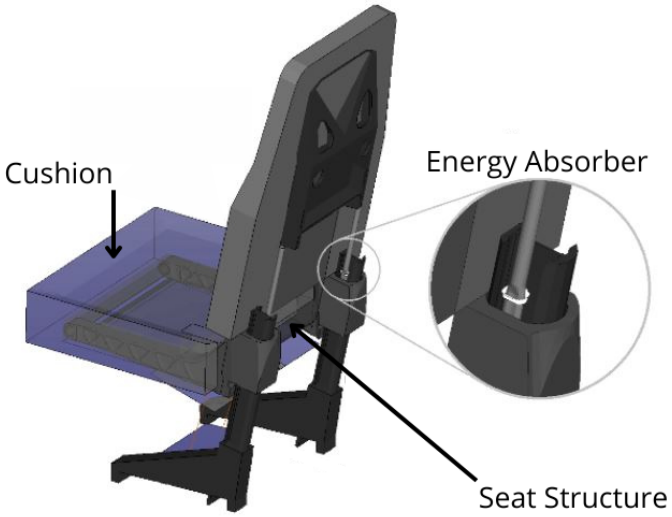

Figure 2.4: Typical Crashworthy Seat Layout, based on Rotorcraft Seats used for Tests in Politecnico di Milano

It consists of several components, each of which influences how the impact load is transmitted to the human body. To conduct a clear and effective analysis, it is appropriate to examine each component individually. In particular, as shown in Figure 2.4, three main elements can be identified: the seat structure with all its attachments, the cushion, and the energy absorber. These components must then be integrated and analyzed together within a complete seat system, aiming to achieve an optimized configuration that minimizes the risk of severe injury to the occupant.

2.4. The Influence of Energy Absorbers

An energy absorber is a component designed to reduce the energy transferred to the body of a passenger or pilot during an impact or sudden deceleration, such as in the case of an emergency landing or accident. These devices aim to minimize the risk of injury by reducing the force applied to the human body.

The principle of operation of an energy absorbing device is based on its ability to dissipate kinetic energy during an impact. The typical method of energy absorption involves the dissipation of most impact energy through the crushing and deformation of a system. Generally, a longer stroke of the energy, absorbing device before bottoming out results in a lower lumbar load curve. However, there are multiple energy absorption (EA) solutions described in the thesis [11]. For completeness, below is a list of the most common solutions mounted on rotorcraft.

- Crushable column
- Inversion tube
- Tube and die or roller
- Wire or rod bender
- Deformable link
- Hydraulic
- Pneumatic

Rotorcraft seats are equipped with energy absorbers (EA) since, without them, rotorcraft seats would not meet crashworthiness regulations, which require higher g-forces compared to those prescribed for aircraft. However, although not mandatory or essential to meet the regulatory requirements, EAs can also be applied to certain types of aircraft.

To better understand the effectiveness of energy absorbers in reducing lumbar load, the results obtained in the following study from the Politecnico di Milano can be analyzed [12]. A previously validated numerical model, developed using a multi-body technique, provides interesting results regarding lumbar load in three different scenarios: using a rigid seat, using a seat equipped with energy absorbers, and using a seat equipped with energy absorbers characterized by a reduced available stroke.

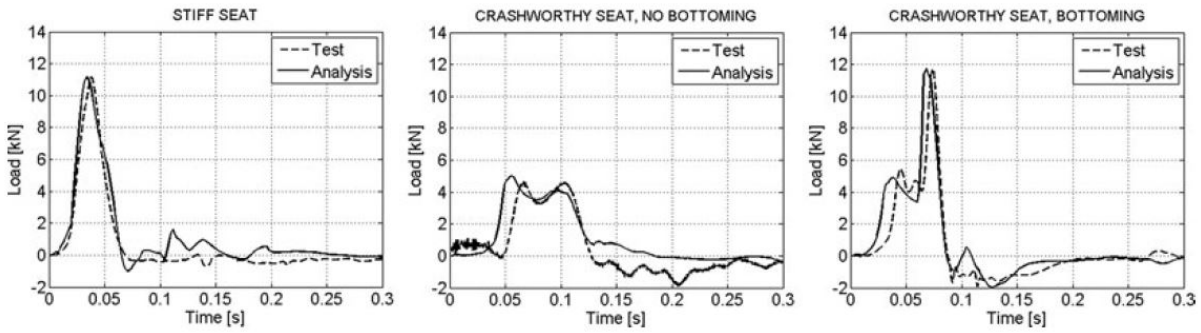

Figure 2.5: Comparison of Lumbar Load associated with a Rigid Seat, a Seat with an Energy Absorber (no Bottoming), and a Seat with an Energy Absorber with a Reduced Stroke (with Bottoming).

As shown in Figure 2.5, a well-functioning energy absorber significantly reduces the lumbar load on the occupant compared to a rigid seat. However, an energy absorber that bottoms out with a reduced stroke may, in fact, increase the lumbar load.

2.5. The Influence of the Cushion

Seat cushions have been the subject of extensive research due to their crucial role in ensuring passenger comfort without exceeding the maximum spinal load during impact events. Depending on the type of aircraft and specific operational requirements, different types of cushions are utilized. The first and most important consideration is discussed in [13].

A qualitative correlation between lumbar load and cushion characteristics, particularly the load-deflection curve and cushion thickness, suggests the existence of a specific load-deflection profile that maximizes lumbar load for a given thickness. This means that, for a fixed cushion thickness, both softer and stiffer curves than the critical one will result in a lower lumbar load than that corresponding to the critical curve. Consequently, it is not possible to determine a priori whether a softer or harder cushion will minimize lumbar load.

Two conceptual experiments are proposed to clarify this idea.

The first involves a dynamic test, compliant with CS-25.562 regulations, employing a 14 g acceleration pulse and a rigid iron seat without any cushion. In this configuration, the lumbar load remains well below 4400 N, settling at just over 4000 N. The load-deflection curve of the rigid seat lies above all possible cushion curves. These observations indicate that lumbar loads associated with cushion load-deflection curves stiffer than the critical one (which gives values of 4400 N) asymptotically approach the rigid seat value, approximately 4200 N.

The second scenario considers the same dynamic test performed with an extremely soft cushion placed on top of the same iron seat. This cushion is so compliant that it fully compresses under the occupant's weight, producing a load-deflection curve that lies below any realistic cushion profile. In this case, the cushion behaves almost like the rigid support beneath it, again resulting in lumbar loads approaching $4200; N$, asymptotically approaching $4000; N$.

This analysis confirms that lumbar loads corresponding to curves either stiffer or softer than the critical one tend to converge toward $4400; N$, implying that the peak lumbar load observed when using a cushion will always exceed the $4000; N$ of the fully rigid configuration.

This conclusion is further supported by both experimental and numerical findings from a study conducted at the Politecnico di Milano [14], which aimed to characterize the

mechanical response of various cushion types. Cushions of different foam materials and thicknesses were tested under both static and dynamic conditions to define their individual load-deflection curves. The results corroborated the theoretical expectations outlined above.

Ideally, the entire kinetic energy of the occupant should be absorbed by the cushion without generating a force that exceeds the regulatory lumbar load limit. However, as previously discussed, the interaction between the cushion and the occupant's soft tissues can amplify upper body deceleration, thereby increasing spinal loading. As a result, stiffer cushions are often chosen to keep lumbar forces within acceptable limits, though this typically comes at the cost of reduced comfort.

Among the most commonly used materials for seat cushions are polyurethane foams [15] [16], which are complex polymeric materials produced by the reaction between isocyanates and polyols. These foams can be engineered to exhibit a wide range of properties, from low-density, flexible foams to high-strength elastomeric castings.

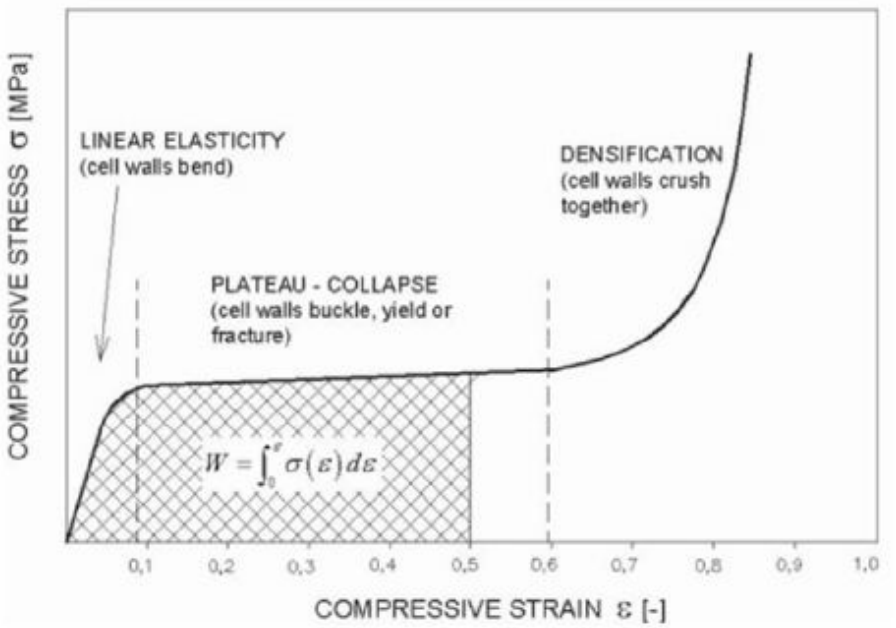

Figure 2.6: Typical Stress Strain curve for polymeric foam

As shown in Figure 2.6, under compression, polyurethane foams generally exhibit three distinct mechanical regimes:

- Linear regime: At low strains, the foam behaves elastically, with the internal struts bending under load.

- Plateau regime: As strain increases, the struts begin to buckle, resulting in a near-constant stress response.
- Densification regime: Once the struts are fully collapsed, stress increases sharply with further strain.

Moreover during unloading, the stress response is lower than during loading. The area enclosed between the loading and unloading curves represents the hysteresis, which quantifies the energy dissipated during a load cycle. Therefore, ongoing research seeks foams with high plateau stresses (despite reduced comfort) and elevated hysteresis values to enhance energy dissipation.

A promising alternative to extremely stiff foams is the class of strain-rate-sensitive foams, such as those commercially known as Confor [17]. These materials exhibit increasing stiffness with increasing compression rate, offering a comfortable experience during normal operation while providing high energy absorption during crash scenarios. In contrast to low-rate-sensitive foams, high-rate-sensitive foams behave more like a combination of a damper and a spring, rather than a simple spring. During impact, these materials convert part of the kinetic energy into heat, resulting in significant hysteresis losses. This energy dissipation is reflected in the load-deflection behavior, which shows a marked difference between the loading and unloading phases. The typical behavior of the two materials is shown in Figure 2.7 below, demonstrating how Confor's properties make it more suitable to fulfill the desired performance requirements.

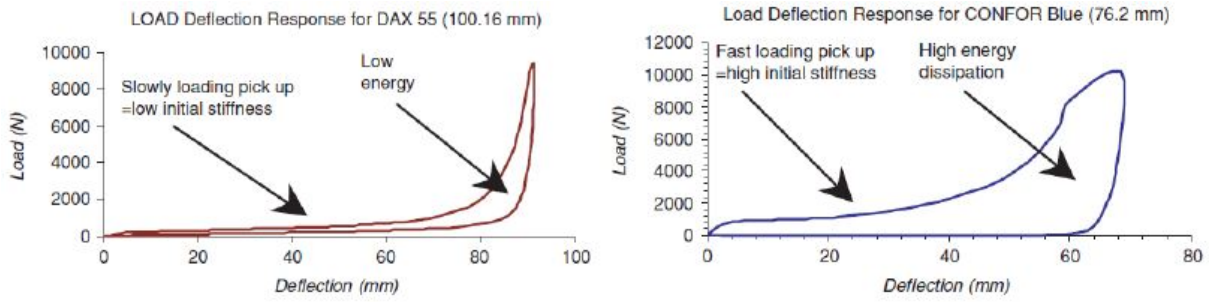

Figure 2.7: Comparison between the Stress-Strain Curve of a Polymeric foam and Confor

2.6. The Influence of the Seat Stiffness

As explained in the previous Paragraph 2.5, a completely rigid seat is the one that reduces lumbar load on the passenger the most. However, in reality, it is impossible to build a truly rigid seat. In fact, the materials used in civil aeronautical seats, combined with the seat structure, the connections between the seat and the aircraft, the internal connections

within the seat itself, as well as the seat's wear and tear over time, can result in a wide range of overall stiffness values.

It is therefore relevant to understand the influence that the seat's stiffness has on lumbar load. In fact, different stiffness levels can lead to varying degrees of dynamic coupling with the occupant's body, that is, the degree of interaction and energy transfer between the seat and the human body during an impact.

The previous thesis conducted at the Politecnico di Milano [18], which forms the starting point of this work, investigated this topic. A numerical FEM model was developed and validated using experimental test data, and it confirmed the expected trend: the peak lumbar load decreases as the seat stiffness increases, reaching its lowest values when the seat approaches a nearly rigid configuration.

2.7. Aim of the Work

Based on this literature review, it is now possible to clearly outline the objectives of this thesis.

Unlike in [18], where a finite element method (FEM) approach was adopted, this work employs a multi-body numerical model to offer a different perspective on the same problem. The first objective was therefore to investigate the same topic addressed in [18] by developing a functional multi-body model. This was achieved by comparing the simulation results with those from a previously conducted experimental campaign, in which different seat stiffness levels, representing the variability that may arise due to the factors discussed in Section 2.6, were modeled using four springs mounted beneath the seat. To verify the consistency of the previous experimental data in the no cushion configuration, two additional tests were carried out using two types of die springs 3.2.4 selected from those employed in the experimental campaign conducted for the present thesis.

Once reliable and consistent results were obtained with the multi-body model, further tests were carried out to introduce the cushion as an additional variable. Although seat cushions have been widely studied as standalone components, it is of considerable interest to explore the interaction between cushion properties and seat stiffness when analyzed in combination. In this second phase as well, the experimental data were used to validate the multi-body model.

This modeling approach enables a fast and effective analysis of the phenomenon, ultimately supporting the development of the final conclusions.

3 | Experimental Activity

3.1. The lab LaST

All experimental tests conducted for this thesis were carried out at the Laboratorio per la Sicurezza dei Trasporti (LaST), located on the Bovisa Candiani campus of the Politecnico di Milano. The laboratory is part of the Department of Aerospace Science and Technology and has been active in the field of passive safety since the 1960s. Its mission is to improve passive safety in the transport sector by combining numerical simulation techniques with experimental testing. The laboratory is equipped with a crash test sled, various drop test machines, high-velocity impact launchers, and several systems for static testing.

The tests relevant to this thesis fall within the category of deceleration tests, which focus on components, such as seats, that are not directly involved in the impact itself but are subject to its transmitted effects. To perform this type of testing, several specific components are required, which will be presented in the following paragraphs.

3.2. Test Components

3.2.1. Sled and Braking System

The Laboratory's facility used for the dynamic tests consists in a 54-meter-long deceleration sled. The sled is initially accelerated in a controlled manner by a compressed air system until the target velocity is reached. The braking phase is achieved through a custom-designed deceleration system consisting of multiple steel rods placed transversely across the track.

As the sled moves forward, it engages the rods, dragging them along its path. This process causes the rods to stretch and deform, thereby absorbing and dissipating the sled's kinetic energy. To shape the deceleration profile as required by regulations, the rods are pre-deformed at specific positions, allowing them to engage with the sled at different moments throughout its travel. Additionally, the ends of the rods are trimmed

to varying lengths. This ensures that, once deformed and dragged by the sled, they detach from the braking system at staggered intervals, thereby progressively modulating the braking action over time.

The preparation process of the steel rods is as follows. First, two pre-deformations are applied using hydraulic pistons to allow the correct positioning of the rods within the braking system rollers. Then, three rods at a time are pre-deformed using a larger hydraulic piston. Steel profiles are properly positioned to engage the rods and deform them differentially, elongating them by the desired amount. This process is repeated until the correct sequence of nine rods is obtained. Once the rods are prepared, the ends are trimmed with a grinder to the required length to enable their sequential disengagement from the braking system. A new set of rods was manufactured for each test to ensure proper braking of the sled.

The preparation details for the steel rods, starting from the dimensions used in the previous experimental campaign and following an analysis of the forces involved as well as a settling run, were slightly modified and are as follows:

N. of Rods	Pre-Deformation [mm]	Cut [mm]
1	1000	/
2	1090	/
3	1220	340
4	1330	220
5	1430	150
6	1500	70
7	1560	45
8	1580	30
9	1600	20

Table 3.1: Rods Details

It must be noted that the deceleration profile cannot be perfectly reproduced across different tests, nor can the ideal profile be exactly achieved. In fact, despite the careful preparation of the steel rods, the sled may reach the impact at slightly different speeds, and the rods themselves may become engaged differently or behave slightly inconsistently between individual rods. Therefore, even when regulatory requirements are met, variations in the deceleration profile between tests will inevitably influence lumbar load results. Nevertheless, as long as the profiles remain within the prescribed limits, the tests can still be considered comparable. Figure 3.1 shows the sled and braking system used.

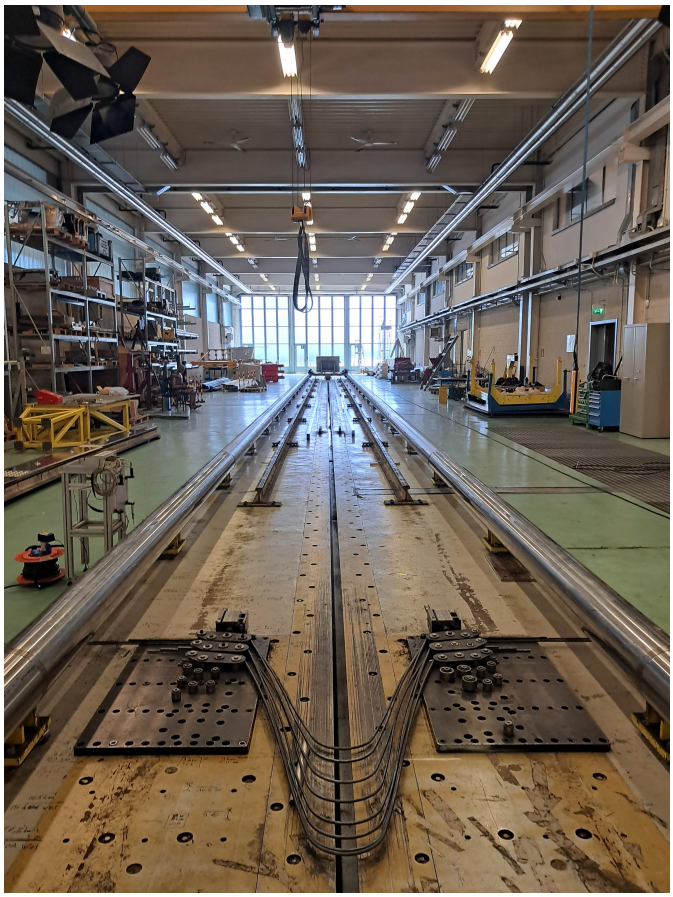

Figure 3.1: Sled System

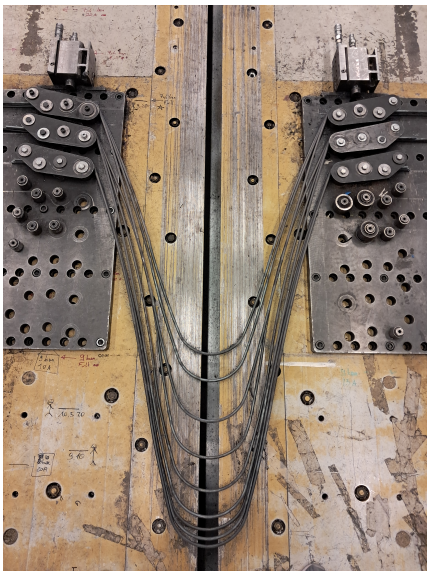

(a) Before Sled Braking

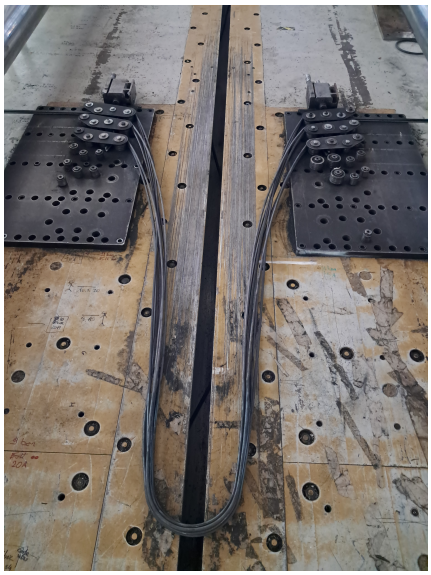

(b) After Sled Braking

Figure 3.2: Braking System

3.2.2. Seat

The seat previously manufactured was designed for experimental and research purposes. It complies with several design guidelines presented in [6] [19]; for instance, it features a seat pan inclined at 8°, satisfying the requirement of being greater than 5°, and a backrest inclined at no less than 12°. The seat surface measures 42×37 *cm*, while the backrest height is 62 *cm*.

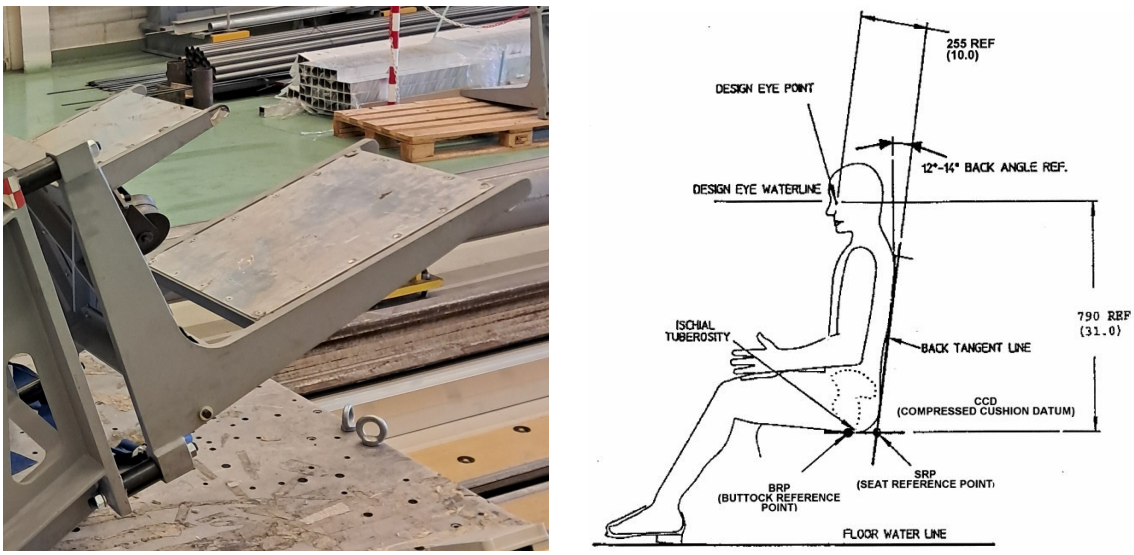

(a) Test Seat (b) Seat Requirements

Figure 3.3: Seat

However, to simulate full rigidity under test conditions, the seat was entirely constructed from steel, resulting in a highly resistant structure. This design choice led to a total mass of 50 *kg*, which is not representative of an actual aircraft seat. Nevertheless, the position of the center of gravity is consistent with that of a real seat, allowing the model to be scaled accordingly to match the mass of a real seat, as will be explained in Chapter 7.

Finally, the seat is equipped with a two-point seatbelt, directly attached to the seat structure. Once the ATD is positioned, the belt is adjusted through the buckle in order to properly restrain the dummy during the test.

3.2.3. Dummies

The development of crash test dummies began around the 1970s, with the aim of replacing human volunteers and cadavers in impact testing. A crash test dummy, technically referred to as an Anthropomorphic Test Device (ATD), is a full-scale model designed to

replicate the dynamic response of the human body during a crash event. Over the years, increasingly sophisticated and accurate models have been developed to represent different human body types across a wide variety of impact scenarios. Regardless of the specific application, dummies must meet several essential requirements to provide meaningful and reliable results [20]:

- Biofidelity: the degree to which the dummy replicates the biomechanical behavior of the human body during an impact. This allows for the extrapolation of relevant quantities, enabling the calculation of injury criteria and the identification of the most vulnerable body regions. Biofidelity is achieved by designing dummies with masses and inertial properties closely matching those of the human body, for example by replicating the same range of motion associated with specific joints. The foundation for achieving biofidelity comes from measurements taken on human volunteers and cadavers.
- Repeatability: the ability to obtain consistent measurements under identical test conditions. Dummies are particularly valuable in minimizing result variability, as they are standardized, verified devices that remain constant across tests.
- Reproducibility: the ability to achieve comparable results when the same experiment is repeated under different conditions, such as using different laboratories or measuring instruments.
- Durability: the ability to withstand repeated tests without degradation. Dummies are especially useful in high-risk scenarios where the use of human volunteers would be unethical or impossible.
- Standard Calibration: ATDs are periodically calibrated according to regulatory standards (e.g., CFR or ECE) to ensure accuracy and consistency in test results.

Dummies can be equipped with a variety of sensors, the most common of which are load cells and accelerometers, strategically positioned in specific regions of the body as prescribed by testing protocols.

The ATD used in the experiments is a Hybrid II 50th percentile male dummy (Figure 3.4), designed to represent an average adult male with a height of 175 cm and a weight of 74 kg. Although Hybrid II is an older generation compared to the more advanced Hybrid III, its use is justified by the superior design of its lumbar region. For this reason, Hybrid II is still widely adopted in aeronautical crash testing and is the ATD specified by the FAA/EASA for compliance with aviation safety regulations.

Figure 3.4: Hybrid II 50th Percentile

3.2.4. Springs

As previously mentioned, the goal of using compression springs is to simulate the different stiffness levels that a seat may exhibit due to construction materials, joints, and wear. For this reason, the springs are, in theory, expected to operate within the elastic range during dynamic tests.

In the previous study [18], seat stiffness values ranging from 104 N/mm to 3200 N/mm were investigated. However, several interesting observations emerged. Firstly, stiffness values higher than 2000 N/mm tended to behave almost identically to a completely rigid seat. Secondly, difficulties in achieving test repeatability were reported, likely due to work hardening experienced by the springs after the impact tests, which generate extremely high loads in very short durations. In fact, once the material exceeds its yield point and enters the plastic range, the force-displacement curve is altered. As a result, in subsequent tests, the maximum deflection experienced by the spring under the same maximum load as in the first dynamic test will be lower. A lower spring deflection corresponds to a higher lumbar load. Another consideration was made regarding the lower limit of the stiffness values to be investigated. The 104 N/mm spring likely reached its stroke limit during previous tests, and by fully bottoming out, it caused a high peak in lumbar load.

The springs used in the earlier study included round-wire helical springs for stiffness values below 500 N/mm, and disc springs for stiffness values above 500 N/mm.

Given the issues encountered, particular attention was paid to the selection of springs, which ultimately led to the choice of die springs. These are helical springs made from rectangular-section wire, which gives them their unique properties. The cross-sectional area of a die spring is greater than that of a standard round wire spring, and the increased mass of the wire provides higher force. This geometric difference results in rectangular-

wire springs having greater elastic force and increased resistance to deformation and breakage compared to their round-wire counterparts. Die springs are particularly well-suited for high-load scenarios with spatial constraints, as in the case of this thesis. Their compact design allows installation into holes or onto shafts, while still meeting the demands of high-speed compression and heavy loads. As presented in a study by the Associazione Nazionale Costruttori Componenti Elastici Meccanici (ANCCEM) [21], for the same dimensions, springs with rectangular wire exhibit lower deflection and slightly lower corrected stress compared to round-wire springs.

The springs were therefore selected from the Mollificio Bordignon catalogue, in order to meet both the estimated load requirements and the spatial constraints of the test setup. The dimensional constraints required a free length of 70 mm, a minimum internal diameter of 20 mm,, and a maximum external diameter of 60 mm,. Regarding stiffness, the lower limit was raised to K = 209 N/mm, and the upper limit reduced to K = 1980 N/mm.

Additionally, an estimation of the maximum load the springs would have to withstand was conducted by summing the mass of the dummy's upper body and the mass of the seat, and applying the prescribed acceleration from the regulation (in addition to gravity), projected along the Z-axis in the direction of the springs' compression. This force was then distributed asymmetrically across the four springs, since the two front springs are subjected to a greater load compared to the rear ones. Therefore, the estimated maximum load that a single spring may be subjected to during the test is approximately 5000 N.

The characteristics of the springs used in the tests are reported in Table 3.2 and Figure 3.5 below:

	$\mathbf{L}_o$ $[mm]$	$\mathbf{d}_i$ $[mm]$	$\mathbf{D}_e$ $[mm]$	$\mathbf{S}_2$ $[mm]$	$\mathbf{F}_2$ $[N]$	**b x h** $[mm]$	**K** $[N/mm]$
Blue spring	64	25	50	24	5016	10.9 x 6.0	**209**
Red spring	64	25	50	19.2	7930	11.3 x 7.4	**413**
Yellow spring	64	25	50	16	11344	11.4 x 9.1	**709**
Brown spring 1	64	20	40	9.6	11798	8.4 x 10.9	**1228**
Brown spring 2	64	25	50	9.6	19008	11.8 x 13.4	**1980**

Table 3.2: Spring Characteristics

where the spring parameters are defined as follows: L_0 is the free length, d_i the inner diameter, d_e the outer diameter, S_2 the maximum stroke, F_2 the maximum load, $b \times h$ the wire cross-section dimensions, and K the stiffness.

Figure 3.5: Die Springs

Since each test requires four springs, a total of eight springs for each stiffness value (forty springs in total) were purchased to ensure the use of brand-new components for the tests involving the cushion and to allow for redundancy.

3.2.5. Cushions

The cushions used in this study were sourced from Testori Aero Supply, the same supplier that had provided similar components for two previous research projects [14] [15] conducted at Politecnico di Milano. These earlier studies focused on the simplified characterization and validation of aircraft seat cushions. As described in the referenced documentation, the initial characterization tests were carried out on various cushion specimens (Figure 3.6) (from type A to type H). The nominal dimensions of the specimens were 102 mm in height and 190 mm in diameter.

Figure 3.6: Tested Specimen examples

Testing was performed using a hydraulic press under two different conditions:

- Static curves were obtained at a compression rate of 0.001 m/s with a sampling frequency of 20 Hz.
- Quasi-static (low-speed) curves were obtained at a compression rate of 0.8 m/s with a sampling frequency of 4000 Hz.

However, due to the dynamic nature of the deceleration tests to which the cushions are subjected, additional impact tests were performed using a drop tower to better simulate their behavior under dynamic loading. As shown in Figure 3.7 it was observed [15] that the quasi-static curves obtained with the hydraulic press at 0.8 m/s, where a constant velocity could be maintained, closely matched the results obtained from the drop tower, where maintaining a constant speed was not possible. As a result, the quasi-static curves were deemed suitable for modeling the cushion's material behavior.

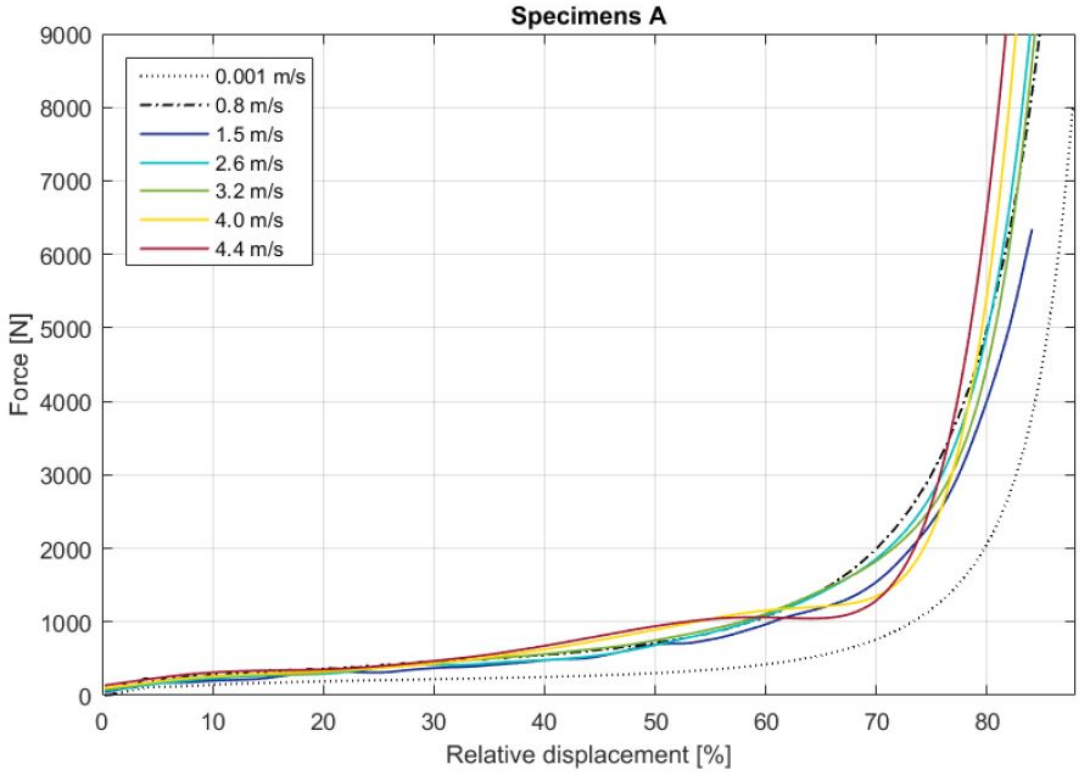

Figure 3.7: Specimen A Characteristic Curves

For the experimental tests carried out in this thesis, type A specimens were used. These cushions consist of three foam layers: 70% FRM C65, 20% FRM C55, and 10% FRM C45.

To scale the test data to actual cushion conditions, the force-displacement curve of specimen A was adjusted based on the effective contact area as explained in Figure 3.8. While the cylindrical specimen had a contact area of 0.0284 m^2, the area in contact between the cushion and the seat, where the ATD applies pressure during testing, was estimated to be approximately 0.08 m^2. A correction factor was therefore applied, based on the ratio between these areas, to derive the effective force-displacement curve of the cushion represented in Figure 3.9.

(a) Cushions (b) Contact Cushion Surface

Figure 3.8: Tested Cushions

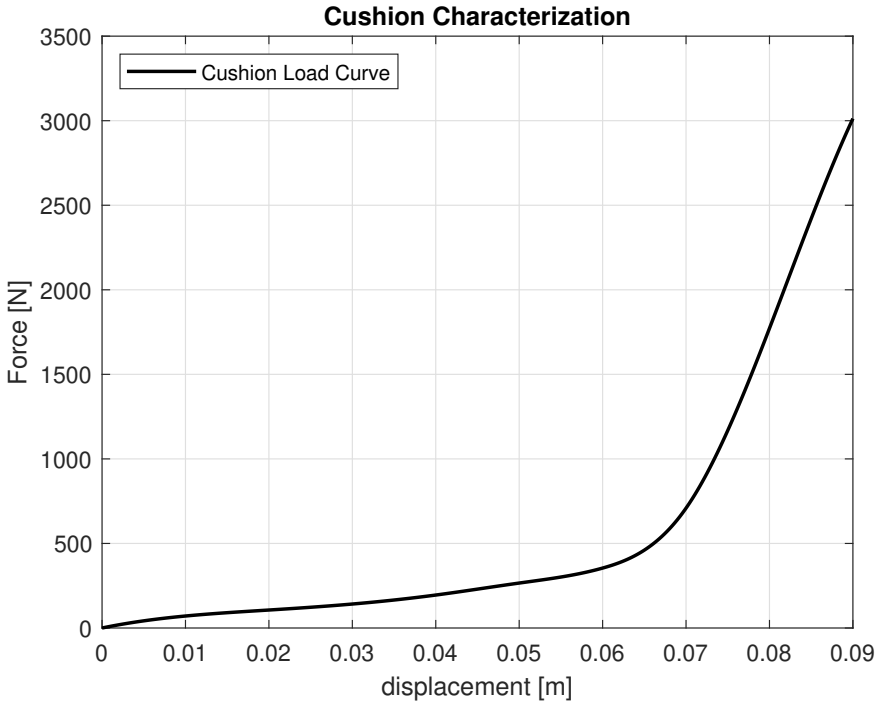

Figure 3.9: Cushion Type A Load Curve

According to the reference document [14], the type A cushion, considering only reliable test results, produced an average lumbar load of 6110 N (Figure 3.10). This value, along with the 4000 N lumbar load recorded with a completely rigid seat without any cushion, is used in this thesis as a benchmark for comparison with the results obtained.

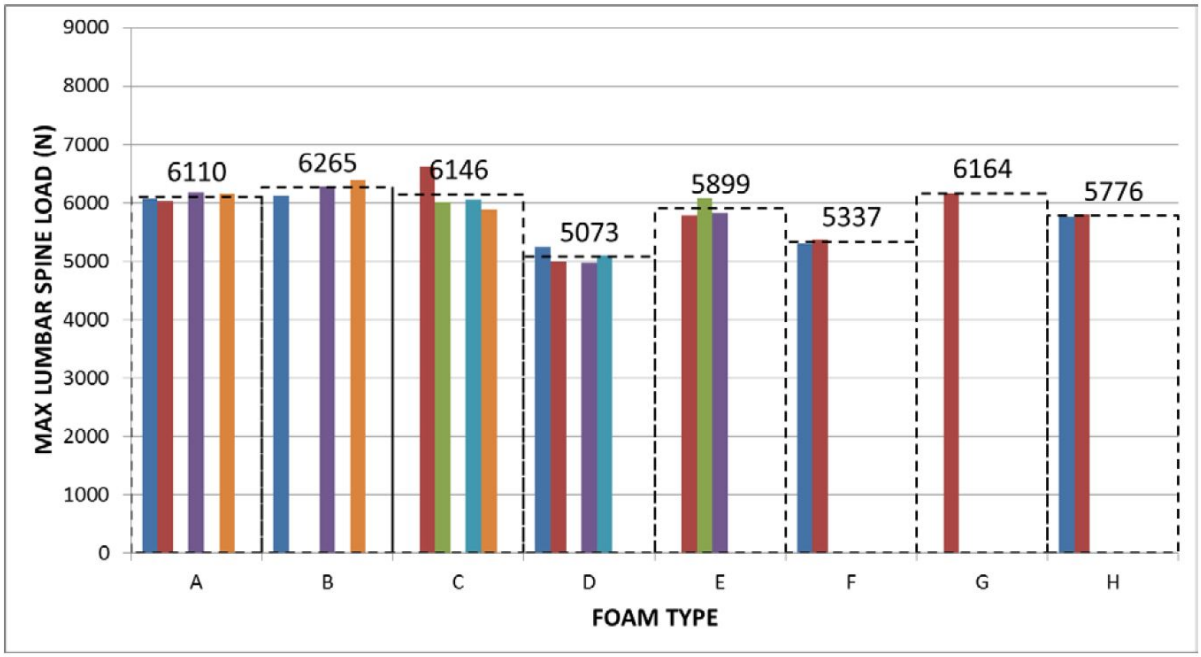

Figure 3.10: Lumbar Load vs Cushion Type

3.2.6. Instrumentation

In addition to all the facilities described in the previous sections, several measurement instruments were employed during the experimental campaign.

To verify the acceleration pulse, the sled was equipped with two accelerometers, which measure the acceleration profile and check its compliance with the regulatory requirements. Two accelerometers were used instead of one to ensure redundancy. A speed sensor was placed at the end of the sled's free run to verify whether the target velocity at the beginning of the deceleration phase had been reached.

Each ATD was fitted with a load cell in the lumbar region to record the time history of the lumbar load. The data acquisition system sampled all signals at 20000 Hz.

Moreover, two Phantom high-speed cameras were used to capture the motion of the springs. This aspect is particularly important, as it enables the observation of spring and cushion behavior during deceleration through video analysis using PCC (Phantom Camera Control), allowing for accurate measurement of the actual spring compression. Additionally, videos of the full test dynamics were recorded using a smartphone to capture the dummy's motion, which was later used as a validation reference for the numerical model.

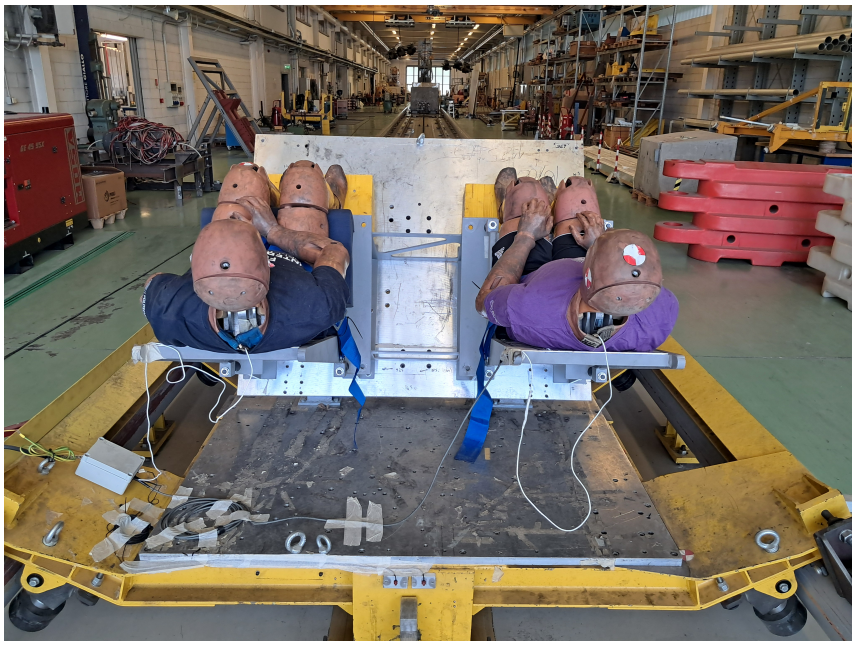

Figure 3.11: Instrumentation setup (Accelerometers and Load Cells)

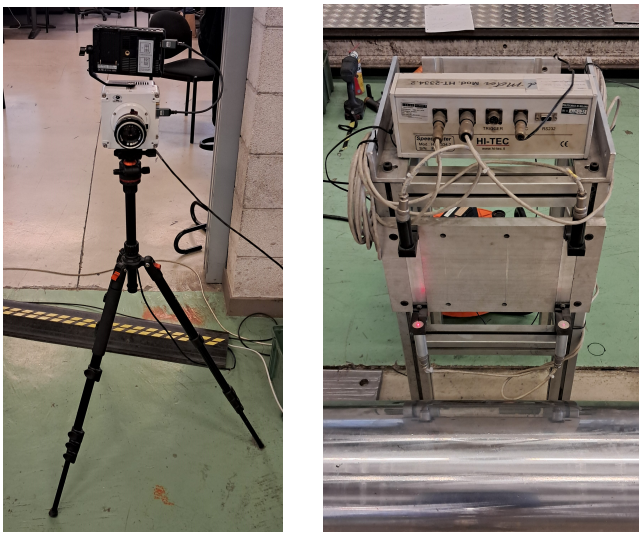

(a) High Speed Camera (b) Speed Sensor

Figure 3.12: Additional Instrumentation

3.3. Test Set-up

The test setup shown in Figure 3.13 follows the procedures outlined in Section 2.2, based on the current regulatory framework [4][5][19]. Since the acceleration pulse on the sled is applied along the horizontal direction, the sled floor and base are tilted 60 degrees

nose-up to comply with the regulations, ensuring that the acceleration vector is applied at an angle of 30 degrees with respect to the aircraft yaw axis.

Although the base is designed to accommodate three seats, only the two outer seats were used to avoid interference between adjacent ATDs. The seats are mounted onto the inclined base using eight custom-made shafts (four per seat), secured with bolts. These shafts also serve to guide the springs, ensuring they operate strictly along their axial direction. For the rigid seat tests, a modification was made to the seat-to-base connection to prevent any seat displacement, effectively simulating a fully rigid configuration. Additionally, wooden boards were placed under the ATDs' feet to replicate the correct floor height.

The ATDs were dressed in simple garments as prescribed by regulations to better replicate a realistic friction coefficient during impact. The dummies were positioned on the seats according to the procedures described in [5] [19], which emphasize the importance of proper ATD positioning: Each ATD shall be placed in the seat in a uniform manner to enhance reproducible results. The ATD should be positioned in the center of the seat, in as nearly a symmetrical position as possible. Initially, the ATD was positioned against the seat backrest with its legs slightly elevated above the seat pan, then gently released to settle under its own weight. However, since the sled moves horizontally and the seat is tilted 60° nose-up, the ATD does not naturally achieve the nominal 1 g preload typically present in a vertical seating configuration. To replicate as closely as possible the hip joint position of an ATD seated under gravity in an upright seat, the dummy was first pressed firmly into the seat by applying force on the shoulders, and then the seatbelt was tightened to ensure firm contact between the pelvis and the seat, thereby achieving a more representative posture. Although no specific regulations are defined for the restraint system, it must be capable of keeping the ATD in position during both the acceleration and deceleration phases of the sled test. Finally, the knees were adjusted to be approximately 100 mm apart, and the hands were placed on the upper thighs just behind the knees.

It is worth highlighting that this procedure was meticulously and personally carried out for each test in order to minimize variability due to setup conditions. Previous studies [22] have shown that the dummy's positioning has a significant impact on lumbar load. While a small tolerance is acceptable in the orientation of the pelvic axes, the pre-load must be applied as accurately as possible. In fact, insufficient initial compression is recognized as a worst-case condition, as it is very likely to result in higher lumbar loads. The referenced document also notes that cushion placement can introduce a certain degree of uncertainty. For this reason, once positioned, the cushion was secured with Velcro straps

and its placement was carefully re-checked before each run.

In conclusion, given the limited number of tests, potential effects of damage or wear on the dummy's pelvis or the cushion due to repeated impacts were considered negligible.

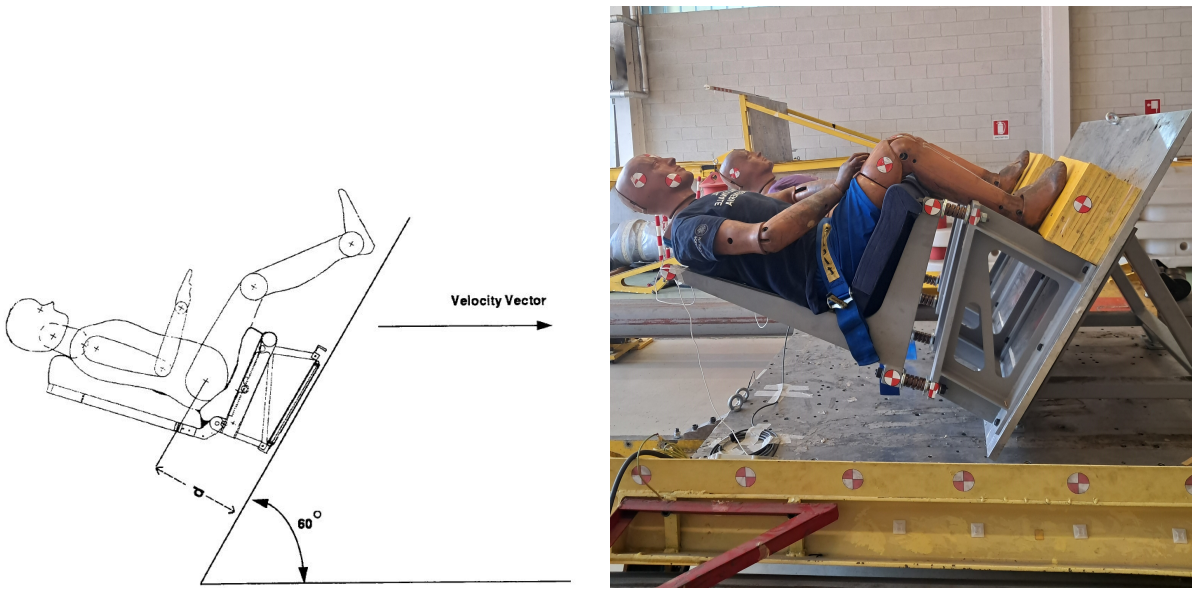

Figure 3.13: Test Set-up

3.4. Test Performed

The experimental campaign was carried out according to the previously described setup and using the materials detailed above. The list of tests performed is reported in Table 3.3 below.

# Test	Seat Stiffness [N/mm]			
	ATD LH Cushion		ATD RH Cushion	
1	Rigid	yes	Rigid	no
2	1980	yes	1228	yes
3	209	yes	413	yes
4	709	yes	1228	yes
5	1980	yes	1228	yes
6	709	yes	413	yes
7	709	no	413	no

Table 3.3: Experimental Tests Matrix

4 | Experimental Results

The initial tests were conducted to verify reference values and confirm results previously obtained in other studies. As a first step, a test was performed with a setup that included one seat entirely rigid without a cushion and another identical rigid seat equipped with a cushion. The results were consistent with expectations, confirming previous findings: the peak lumbar loads recorded were approximately 4000 N without the cushion and 6100 N with the cushion.

A second test was then carried out using the spring-mounted seat configuration without the cushion. Springs with intermediate stiffness were selected to obtain results that did not lie at the extremes of the investigated stiffness range. These tests were specifically aimed at comparing the results with those reported in the reference thesis [18]. The outcomes demonstrated that, despite using slightly different springs and conducting the tests four years after the original campaign, the results remained comparable. Consequently, the previous data were deemed valid for the purpose of validating the multibody model without a cushion developed in this work.

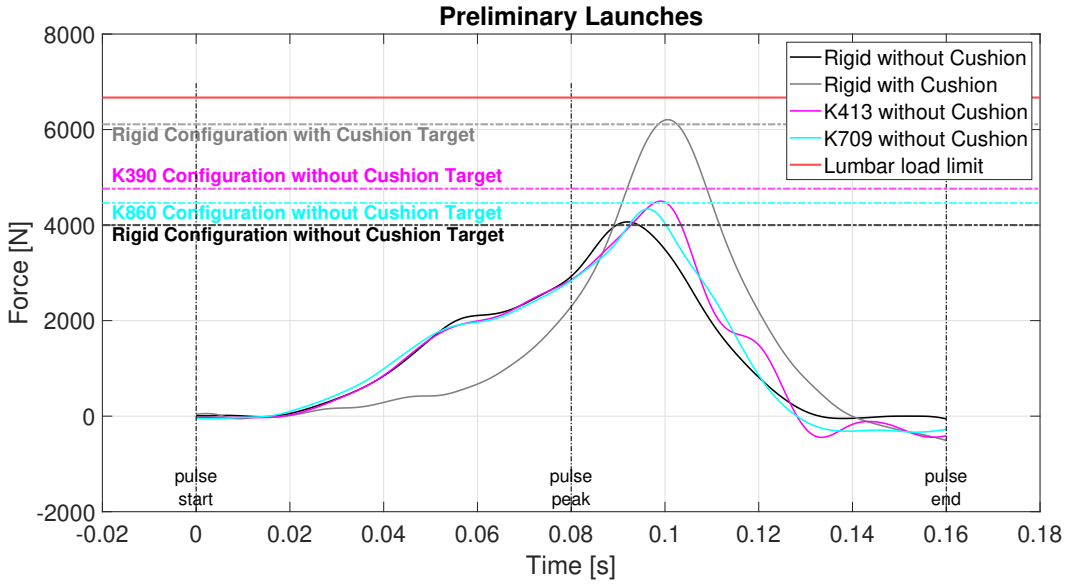

Figure 4.1: Setup Verification and Pre-Test Runs

Following this verification phase shown in Figure 4.1, the experimental campaign focused on the configuration of interest for this thesis: the seat equipped with both springs and a cushion. The results obtained are presented below in Figures 4.3 4.3:

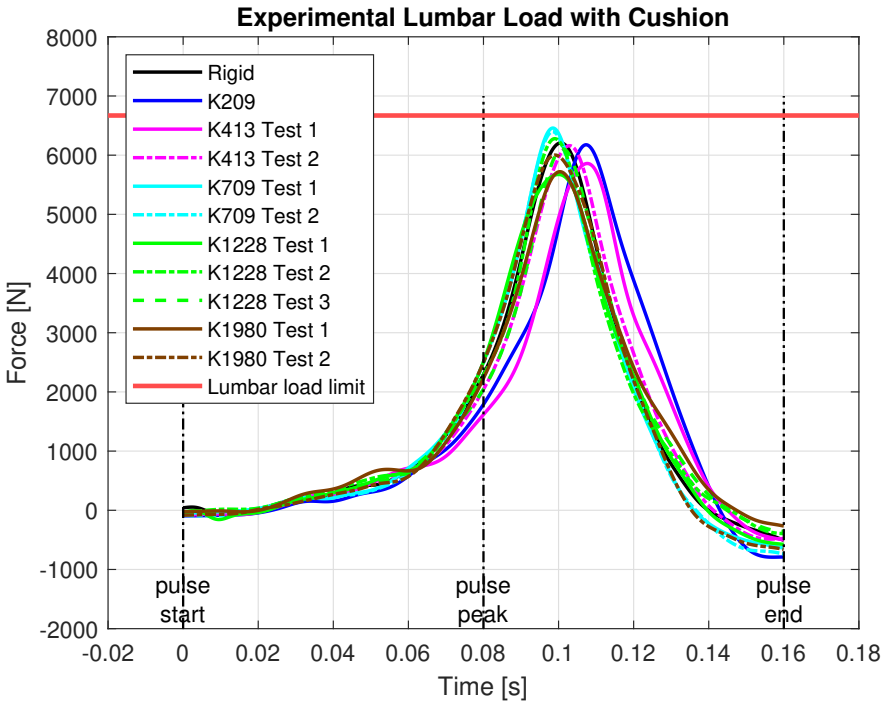

Figure 4.2: Comparison between the Experimental Lumbar Load Time Histories

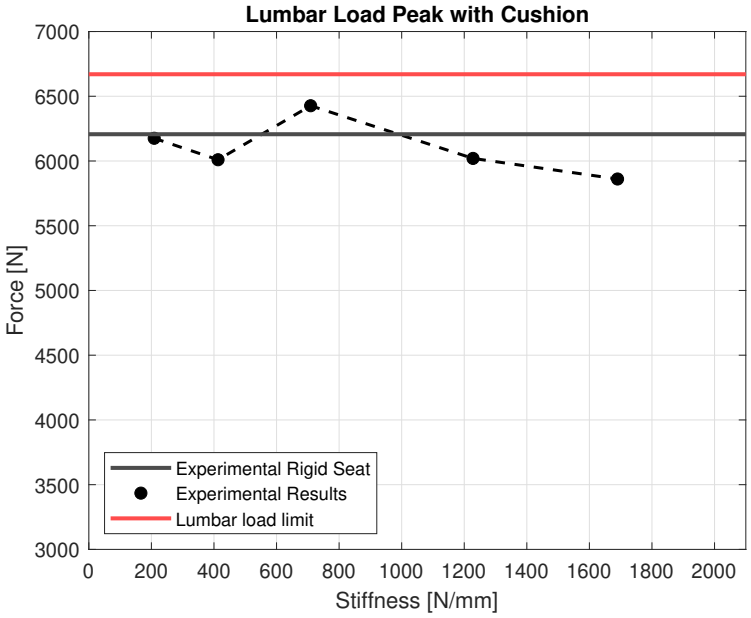

Figure 4.3: Comparison between the Experimental Lumbar Load Peak

The outcome of the test campaign is particularly interesting. The first noteworthy observation is that no clear trend can be identified in relation to the different seat stiffness values. This unexpected result was further investigated by closely analyzing the test dynamics. Video analysis revealed that, during deceleration, the spring is compressed primarily by the displacement of the seat alone, while the dummy is initially slowed down by the cushion. As a result, the dummy only comes into contact with the seat and compresses the cushion at its maximum only at a later stage.

In fact, the complete compression of the cushion and the peak lumbar load occur when the springs have already reached their maximum compression. At that point, the springs begin their elastic rebound just as the dummy makes contact. The dummy's arrival maintains the springs in a compressed state for a longer time, but without causing additional deflection. From the video analysis of multiple test runs, it was observed that the time interval between the moment the springs reach their maximum compression and the moment the dummy fully compresses the cushion and the peak lumbar load is recorded is always present and generally shorter for stiffer springs, reaching up to 0.021 s for the softest one. This phenomenon means that the dummy, at the end of its motion, impacts a seat that, due to the pre-compression of the springs, behaves as if it were nearly rigid. As a result, the lumbar load is influenced almost exclusively by the cushion, as evidenced by the peak values and the absence of a discernible trend linked to seat stiffness.

To better clarify this concept, it can be said that the cushion effectively decouples the influence of seat stiffness from the dummy's response. This effect is even more evident in the test performed with the 209 N/mm spring. Although this spring, being at the lower end of the investigated stiffness range, was expected to reach maximum travel without bottoming out, it nevertheless experienced slight bottoming out. However, this did not affect the lumbar load, which remained consistent with the other tests involving the cushion and springs that did not reach their compression limit.

This contrasts with what was reported in [18], where the 104 N/mm spring bottomed out completely in the absence of a cushion, generating a lumbar peak of approximately 5800 N. This represented an increase of around 1000 N compared to the K = 390 N/mm case, in which the spring did not bottom out.

It can therefore be concluded that the presence of the cushion completely decouples, or at least renders negligible, the dynamic interaction between the dummy and the seat, as the dynamic coupling between the dummy and the cushion proves to be far more significant.

The two distinct phases clearly visible in the video recordings 4.4 shown below further illustrate this phenomenon.

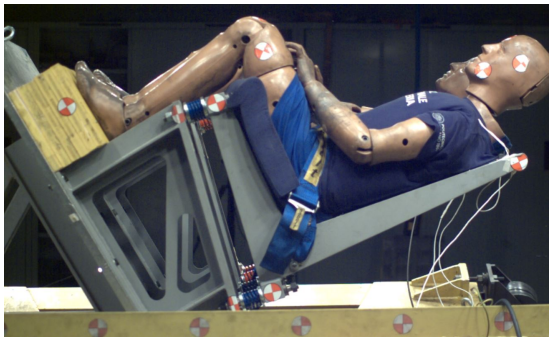

(a) K209, Frame 1169 – Spring bottoms out.

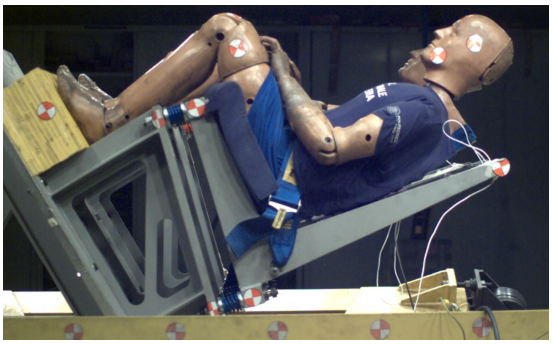

(b) K209, Frame 1236 – Spring fully bottomed for $\Delta t = 0.021$ s; peak lumbar load reached before rebound.

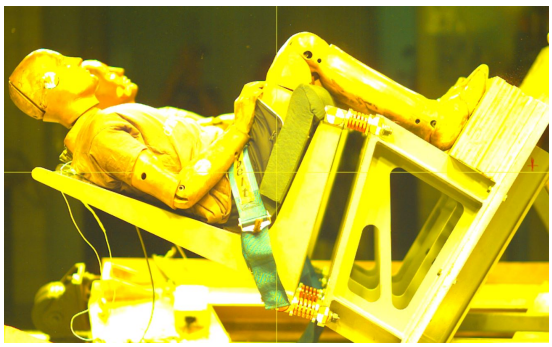

(c) K413, Frame 1171 – Maximum spring compression reached.

(d) K413, Frame 1235 – Spring still fully compressed for $\Delta t = 0.020$ s; peak lumbar load reached before rebound.

Figure 4.4: Experimental Dynamic Video Analysis

Additionally, it is important to note that result variability is also affected by the intrinsic nature of cushion testing; as mentioned in [22] and by the challenges in achieving identical deceleration profiles across different tests. Nevertheless, it is evident that the lumbar load variations caused by changes in seat stiffness observed in the cushionless tests are not present when a polyurethane foam cushion is added.

An additional consideration is that the seat used in the test campaign has a mass of 50 kg and was selected for research purposes; therefore, it is not representative of a typical aircraft seat. The high mass being decelerated clearly affects spring compression. Although it was not possible to validate the model using a more representative mass, it was still considered of interest to investigate how the system behaves when coupled with a 10 kg seat. This scenario will be further explored in Chapter 7.

5 | Numerical Model

Experimental testing plays a crucial role in both the validation of numerical models and the certification of products. However, organizing experimental tests can be challenging, as they are often time-consuming and expensive.

In this context, numerical modelling tools have become increasingly important. Their key advantage lies in enabling optimisation analyses aimed at identifying the best structural solution prior to any physical testing. This allows for a reduction in the number of required tests, and thus, in overall testing costs. A reliable and validated model becomes a valuable resource for research and analysis, enabling engineers to focus experimental efforts exclusively on the tests necessary to satisfy regulatory requirements. Advancements in computational power and the rapid evolution of simulation software have made numerical analyses not only more accurate and repeatable but also significantly faster. When evaluating the passive safety performance of an aeronautical seat, the most widely adopted numerical approaches include [23]:

- Tools based on the Finite Element Method (FEM)
- Tools based on the Multibody (MB) method
- Hybrid or coupled methods, which combine both FEM and MB techniques

The choice between these methods generally depends on the goals of the simulation and the level of detail required for modelling components such as the anthropomorphic dummy, the seat structure, and the restraint systems.

In the multibody (MB) approach, components are represented as rigid substructures connected by kinematic joints, which can interact with deformable elements and contact surfaces. Material and contact properties can be defined to capture key physical behaviours, making this method highly versatile. One of the main advantages of the MB approach lies in its computational efficiency: it requires significantly less CPU time and does not demand a fully detailed structural design. In contrast, the Finite Element Method (FEM) relies heavily on mesh quality and refinement, which greatly impact both accuracy and computational cost. As model complexity increases, a finely meshed FEM model can

become extremely resource-intensive.

Multibody modelling is still widely used in aeronautics, both for preliminary analysis and because of its greater versatility compared to the FEM approach. It proves particularly effective when only an approximate understanding of the system's dynamic response is required, such as during impact events, without the need for fine structural detail. Interaction forces are generally easier to handle in MB models than in FEM ones.

However, the MB approach also has notable limitations. Because structural components are often represented as rigid bodies, the model cannot accurately capture how individual parts deform or contribute to energy absorption. As a result, it becomes impossible to assess which specific areas of the structure are absorbing loads or undergoing significant strain. This limitation reduces the usefulness of the model when detailed local behaviour is important, for example, in crashworthiness or structural integrity studies. Additionally, the modelling phase can be complex, especially when deciding which elements are essential to include in the simulation to properly reflect the phenomena under investigation.

To balance the strengths of both methods, hybrid or coupled MB-FE approaches have been developed. Hybrid models allow certain components typically those where deformation has a limited effect on system dynamics, like dummies, to be modelled with the MB approach, while using FE modelling for the more structurally sensitive parts.

Nonetheless, for the specific goals of this thesis which focuses on evaluating how different parameters affect lumbar loads, the multibody approach was considered the most suitable. The aim was not to model the detailed structural behaviour of the seat, but rather to allow for an effective and targeted investigation of the phenomenon itself. In this context, the MB model offered the right balance of simplicity, flexibility, and efficiency. In fact, the validated MB model enabled the same simulations as those performed in the FEM-based reference thesis [18] to be completed in approximately four minutes per run, whereas the previous FEM simulations required several hours. This considerable reduction in simulation time allowed for a broader and faster exploration of the parameter space, without compromising the reliability of the insights gained.

5.1. MADYMO

MADYMO (MAthematical DYnamic MOdel), originally developed by TNO (Netherlands Organisation for Applied Scientific Research) and now distributed by Siemens Digital Industries Software, is a computer simulation software designed to analyze the dynamic behavior of physical systems, with a particular focus on vehicle collisions and occupant

injury assessment. Although originally developed for car crash studies, MADYMO has proven to be highly versatile and is now widely employed to simulate impacts involving various modes of transport, including trains, aircraft, motorcycles, and bicycles.

The software combines the capabilities of multibody dynamics, for simulating the overall motion of systems composed of interconnected bodies, and finite element analysis, for modeling the structural response of components. Simulation models can be built using only multibody elements, only finite element components, or a combination of both.

Madymo includes a wide range of Anthropomorphic Test Devices (ATDs) and Human Body Models (HBMs), which can be selected according to the specific scenario and analysis requirements. It enables comprehensive evaluation of various occupant restraint systems, such as seat belts and airbags, across multiple impact configurations: frontal, lateral, rear, vertical, and more complex cases like rollovers.

Models in Madymo are defined using an XML-based input structure organized as a hierarchical tree, in which parent elements are linked to their respective child elements. The following section presents how the multi-body (MB) model used in this study was constructed. All information, implementation choices, and features used in the numerical model developed for this thesis are in full accordance with the official MADYMO user manuals and documentation [24] [25] [26] .

5.2. Multibody Model

As a first step, it was necessary to define the model environment by setting up the reference coordinate system, the simulation duration, and the time step. Working with a system-based approach, the dummy was introduced, the seat structure was modeled, and the restraint system was integrated. Subsequently, contact interactions and simulation features were configured. Finally, the desired outputs were defined.

Each system is composed of various types of interconnected elements, to which different properties can be assigned, such as geometry, mass, and material. It is also possible to modify their spatial position and to impose boundary and constraint conditions.

The complete model is shown in Figure 5.1, and each of its main systems will be discussed in the following paragraphs.

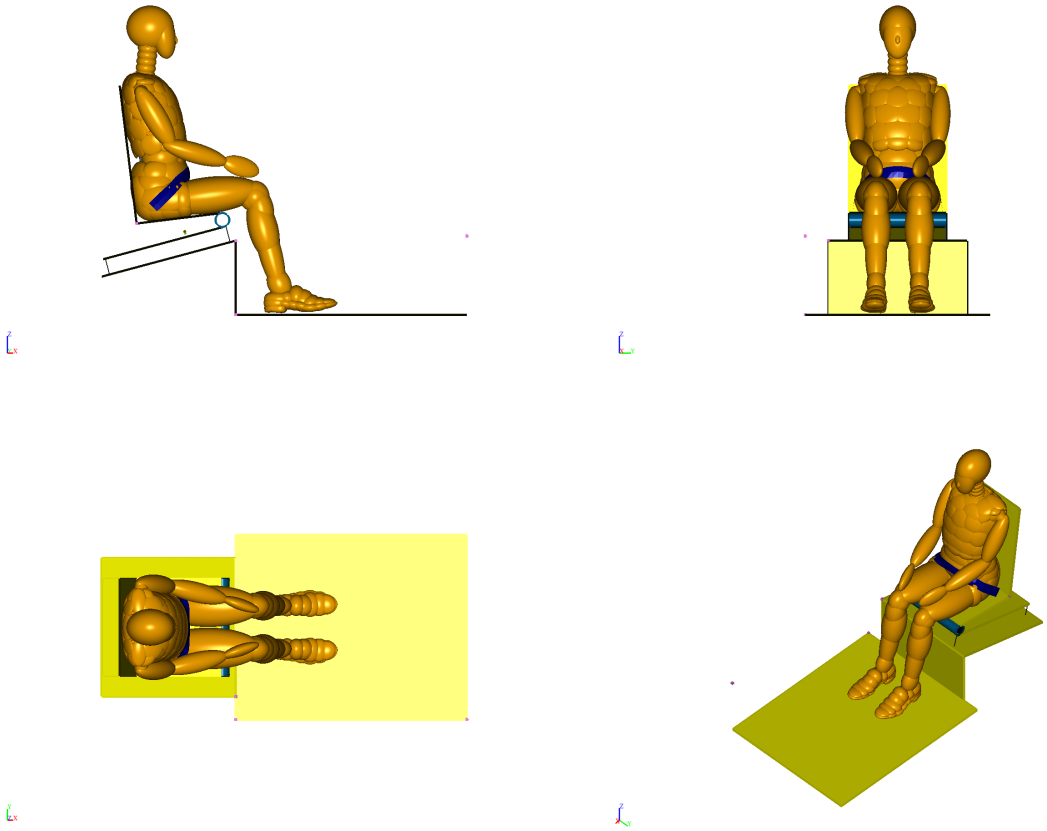

Figure 5.1: Numerical Model Projection View

5.2.1. Seat Model

The seat model was developed based on measurements taken directly from the physical seat and on a previously built LS-DYNA model. Since the seat is designed to behave as a completely rigid structure, its detailed deformation behavior was not of interest; therefore, a simplified geometry was implemented. However, the simplification was carried out while maintaining full fidelity to the key dimensions and surface angles observed during testing.

The seat was modeled using two rigid bodies. The base, which also includes the floor, was made fixed and rigidly attached to the reference coordinate system. The seat body was then connected to the base using a joint, properly oriented. For the simulations involving the rigid seat, a JOINT.BRAC was used, preventing any relative motion between the parts. For the spring-mounted seat configuration, the joint was replaced with a JOINT.REVO_TRAN, which allows translation perpendicular to the base and rotation about the pitch axis. This setup reflects the actual test behavior, where the seat compresses the springs axially and, due to the inertia distribution, loads the front springs

more than the rear ones.

The springs were modeled using RESTRAIN.KELVIN elements, with a CHARACTERISTIC.LOAD function defining a fully linear load-unload behavior to simulate spring stiffness. These restraints were placed at the four mounting points corresponding to the experimental setup, connecting the base to the seat.

The seat itself was geometrically modeled using two SURFACE.PLANE elements to represent the seatpan and backrest. Following the guidelines from Madymo's model database, the seat's thickness was represented by a SURFACE.CYLINDER. This modeling choice addresses a common issue with flat surfaces: when defining contact on a zero-thickness plane like the seatpan, boundary problems may arise, particularly at the edges. A sharp edge can lead to instability or inaccuracies in contact force calculations. By adding a rounded surface, a smoother transition is introduced at the seatpan's end, allowing for more realistic contact with the dummy's legs.

However, it is important to note that some modeling decisions, while not strictly dictated by geometry, can significantly influence simulation outcomes. As shown in this study [27], identifying and optimizing the key design parameters is essential in multibody models. In this case, the vertical positioning of the cylindrical surface was found to have a considerable effect on the lumbar load.

A parametric analysis was carried out to evaluate this influence. When the cylinder was positioned above the seatpan level, it substantially interfered with the dummy's legs, causing them to tilt upward and increasing the lumbar load. On the other hand, lowering the cylinder too much provided insufficient support, allowing the legs to sink excessively into the plane's edge, tilting downward, and again resulting in higher lumbar loads. The configuration that minimized lumbar load and provided the best alignment with experimental data, was the one in which the cylinder was placed flush with the seatpan surface. This setup was therefore adopted for the final model.

Finally, it is worth noting that, when simulating tests with a cushion, the model was kept unchanged except for the surface representing the seatpan. In this configuration, the seatpan surface was assigned the material properties of the cushion, thereby allowing the model to accurately reproduce its physical behavior during the simulation.

5.2.2. Dummy Model

In this work, the dummy used is one of the Hybrid III 50th percentile FAA models available in the MADYMO Reference Database [26]. It is a fully multibody (MB) ellipsoid

model composed entirely of MB parts. This model was selected due to the optimization-oriented nature of the study, where full-MB models offer significant advantages in terms of computational efficiency.

The ellipsoid dummy model comprises 215 bodies, including 50 for the jacket and 6 for the shoes (three per foot). All ellipsoids are interconnected through various joint types, each implemented with appropriate constraints to accurately replicate the motion behavior of individual body segments. These components are encrypted and therefore inaccessible to the user.

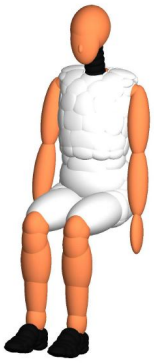

Figure 5.2: Hybrid III 50th FAA Ellipsoid Dummy Model in Reference Position

The model in Figure 5.2 represents a modified Hybrid III 50th percentile male dummy, widely adopted for the development and certification of aircraft seating systems. It is approved by the Federal Aviation Administration (FAA) as an alternative to the Hybrid II dummy for dynamic seat testing under FAR/JAR Parts 23, 25, 27, and 29, as specified in 3.2.3. One of the most notable distinctions between the Hybrid III FAA and standard Hybrid III models lies in the lumbar region, which is particularly well detailed in this version. The lumbar spine is based on the Hybrid II configuration and features both a straight rubber column and an internal steel cable. The rubber column is modeled as a series of rigid bodies connected by joints with limited motion, governed by protected joint resistance models. These models define the compliance of the lumbar spine by describing the relationships between angular (bending and torsion) and linear (compression, elongation, and shear) deformations. The mass and inertia properties of the physical lumbar spine are distributed across multiple MB components. The upper lumbar spine body is connected to the upper torso via a bracket joint, and similarly, the lower lumbar spine body is connected to the lower torso. These bracket joints facilitate the output of constraint loads at the upper and lower lumbar spine load cells. The high level of detail in this area ensures accurate measurement of forces and moments at both ends of the

lumbar spine. The dummy is equipped with multiple sensors, allowing for the extraction of various outputs, including time histories of injury criteria. As the model is already validated, accurate positioning becomes the most critical factor for ensuring simulation fidelity.

The standard method for positioning the dummy begins with the adjustment of its joints. By correctly configuring these joints, both the spatial placement of the dummy and the alignment of its limbs can be set to replicate the experimental setup with high fidelity. In this study, the positions of the arms, hands, legs, and feet were adjusted, and the hip joint was slightly rotated to ensure a proper fit within the seat. An additional crucial step, especially in full-MB simulations, is the use of a settling phase. During this period, the Anthropomorphic Test Device (ATD) is initially placed slightly above the seat and allowed to settle under gravity alone. This ensures that the dummy naturally reaches an equilibrium position before any dynamic loading is applied, thereby guaranteeing that measured loads reflect a realistic seated posture.

5.2.3. Belt Model

The two-point seatbelt was modeled in MADYMO by creating reference nodes corresponding to the attachment points used in the experimental setup. The seatbelt consists of three main segments: a central section modeled with 2D finite elements, and two end segments modeled as 1D multibody (MB) elements, one at each extremity. Material properties were assigned to the finite element portion of the belt, while the load and unload behavior was concentrated in the cable elements through dedicated force-deflection functions. To ensure proper seatbelt performance during the dynamic event, retractors were also modeled. These components were responsible for restraining the dummy during the application of the impact pulse.

Finally, the MADYMO Belt Fitting tool was used to ensure that the seatbelt was appropriately positioned to fit the abdomen and pelvis of the dummy.

5.2.4. Simulation Features

The numerical model was configured by defining the required acceleration fields, contact interactions, and output requests. Contacts were defined between the dummy and the seat cushion and backrest, the feet and the ground, and the seatbelt and the dummy's abdomen and pelvis, each with appropriate friction coefficients and specific contact parameters tailored to reflect the physical interactions observed during the test. The load environment combined gravity with the 14 g crash pulse specified by the regulations 2.2; because the

physical rig is tilted 60 deg, the pulse was decomposed into its X and Z components. The acceleration pulse was applied to both the dummy and the seat, while the base was fully constrained, replicating the deceleration experienced during the sled test. Output data included detailed seat-dummy contact forces for subsequent verification (see Chapter 6.1), the spring elongation and force histories needed to compare the model response with experimental measurements.

6 | Model Validation

Once the model was built, it was validated against experimental data. Specifically, the validation procedure followed the methodology described in this study [28] presented at the 12th International LS-DYNA Users Conference. To validate the model, a series of preliminary analyses were conducted on selected key features and components. Subsequently, the validation process focused on assessing the dummy's kinematics and performing a quantitative comparison between the simulation results and the experimental data.

6.1. Preliminary Check

As a first step, the correct positioning of the dummy was verified. By analyzing the time history of the contact outputs it was possible to evaluate the contact force between the dummy and the seat. In order to achieve a state of equilibrium, this force had to approximately match 600 N.

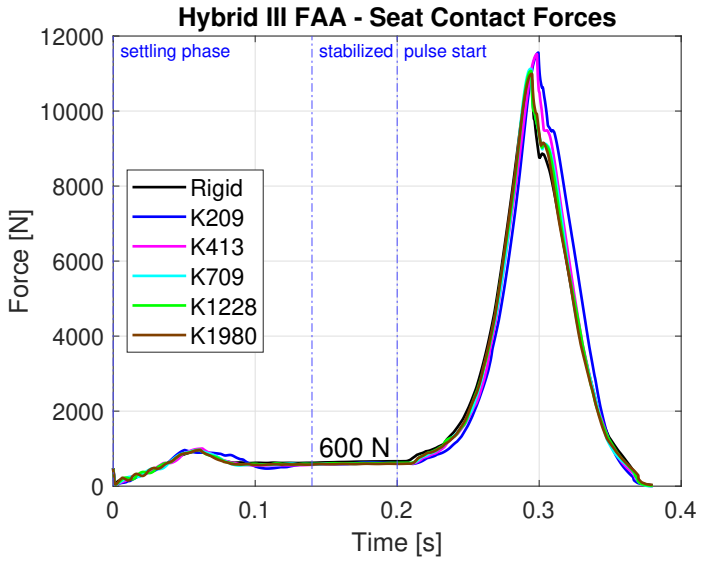

Figure 6.1: ATD-Seat Contact Force Time History

This is justified by the fact that, as can be inferred from the document [29], the masses

of the ATD components acting directly on the cushion, thus significantly influencing the contact, can be estimated to amount to approximately 85% of the total dummy mass. These include the upper part (torso, arms, neck, and head), the pelvis, and part of the thighs. The total mass of these parts is approximately 63 kg, which under the effect of gravity (1 g preload) results in a contact force of around 600 N, consistent with the value reached in the model once the settling phase is completed, as shown in Figure 6.1.

In addition, as a further validation step, the force generated by the impact was analyzed and compared with the theoretical estimate expected from a 14 g acceleration pulse. This comparison was made possible by analyzing the force recorded by the springs, which were modeled using RESTRAIN.KELVIN elements in the simulation. As previously discussed in Paragraph 3.2.4, these springs are subjected to the force resulting from the acceleration of all movable masses. Specifically, the mass of the upper part of the dummy (excluding only the lower legs) was estimated at 63 kg, while the seat contributed an additional 50 kg, resulting in a total effective mass of approximately 113 kg. When subjected to a 14 g deceleration pulse, in addition to gravity, the expected force reaches approximately 16600 N.

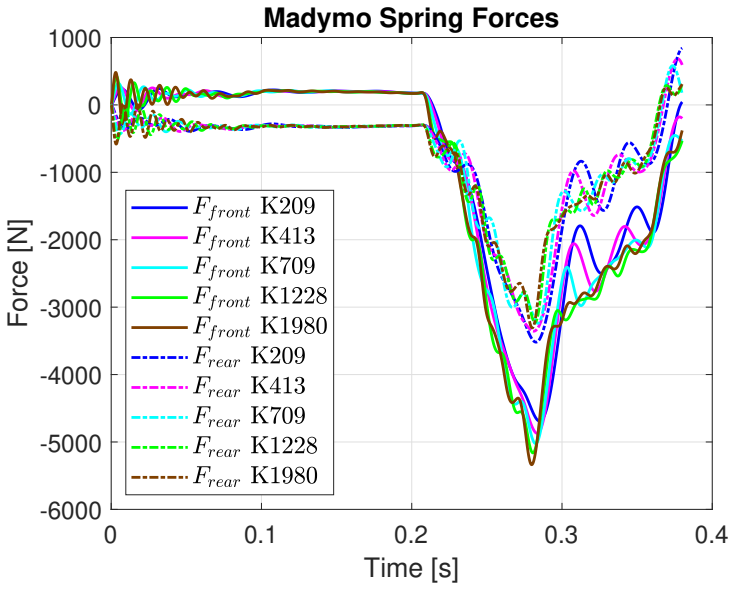

Figure 6.2: Front and Rear Spring Forces

As shown in the Figure 6.2, the results demonstrate good agreement between the numerical model and the theoretical estimation. On average across the simulations, the two front springs each absorbed a force of approximately 5000 N, while the two rear springs each absorbed about 3250 N. This results in a total cumulative load of 16500 N, which confirms the expected value.

6.2. Video Validation

The dummy kinematics from simulation and physical testing were visually compared. Additionally, frames captured at specific time intervals (from pulse start, 0.08 s, 0.16 s, 0.24 s) were used to assess the consistency between the model's motion and the actual test.

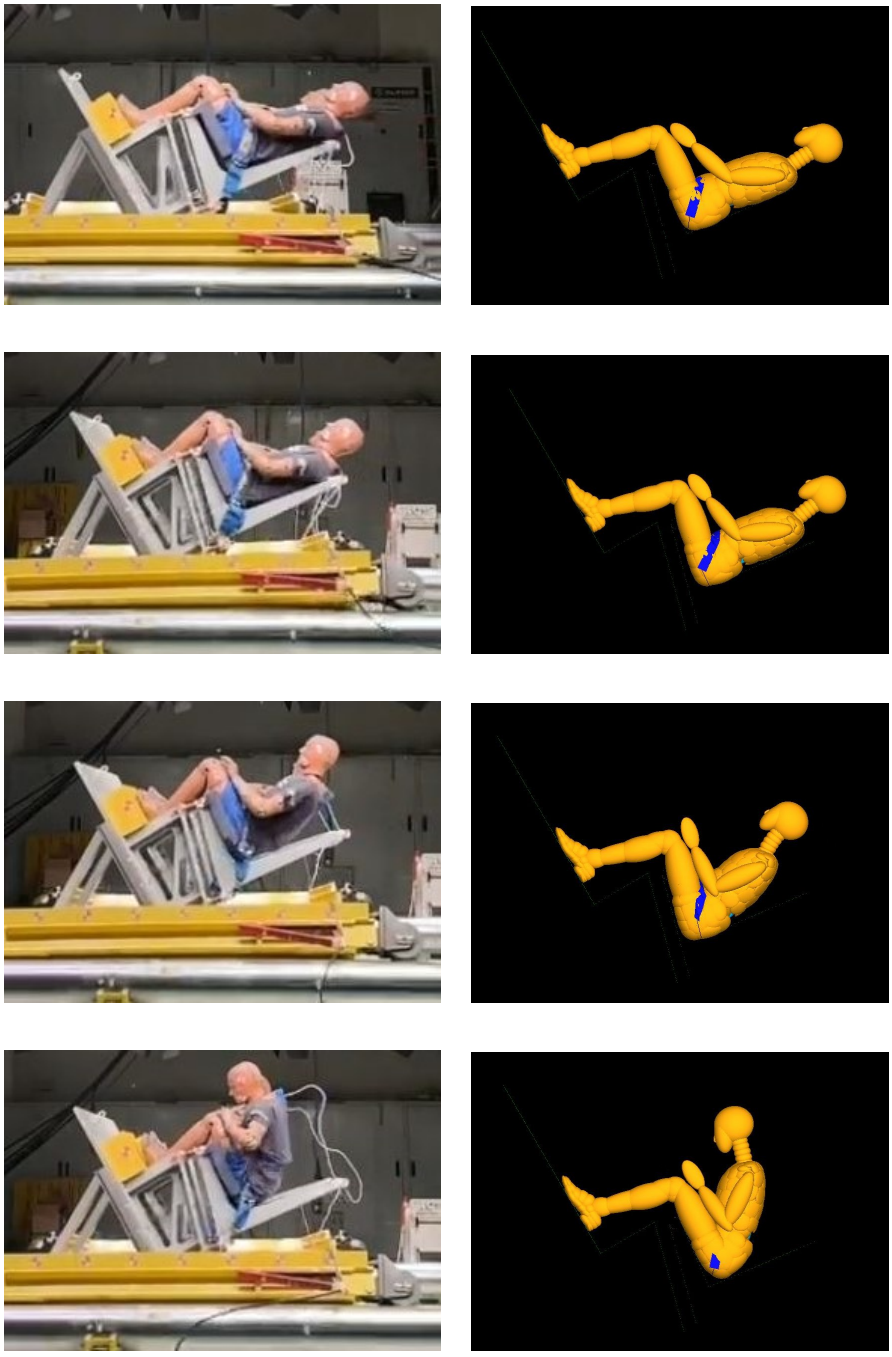

Figure 6.3: Comparison between the Dynamics of Sled Test and Numerical Simulation

The results showed excellent agreement between the simulation and experimental observations. In fact, the dynamics of each part of the dummy were accurately reproduced by the model throughout every phase of the event. In particular, the arms, while interacting with the thighs and partly influencing the lumbar load, remain in a consistent position. At the same time, the two-point belt behaves similarly in both the test and the model, allowing the dummy to load and move forward without completely lifting the thighs off the seat. Finally, the torso appears to visually reproduce the test movements in a symmetrical manner.

6.3. Data Validation

Since this study is centered on lumbar load, the comparison between numerical and experimental data focused on that parameter. The time histories from each test and simulation were examined to verify correspondence in both overall shape and peak magnitude. The curve shape confirms whether the model reproduces the real dynamic behaviour and can therefore be trusted, while the fidelity of peak value is essential to compare against injury criteria 2.1.

An initial qualitative check was followed by a quantitative assessment using the Sprague and Geers metrics [30], which provide separate indices for peak accuracy and curve shape correlation. This method calculates three coefficients to evaluate the level of agreement between two curves: M_{SG} quantifies the accuracy of the peak value, while P_{SG} assesses the fidelity of the overall shape, both of which can be interpreted as percentage deviations. Finally, C_{SG} combines the previous two to express the overall correlation between the curves, where a value of 1 indicates perfect alignment. This coefficient is particularly meaningful, as it provides a single measure of the overall similarity between the curves under analysis, accounting for both the shape affinity and the agreement in peak values.

$$M_{SG} = \left| \sqrt{\frac{\sum c_i^2}{\sum m_i^2}} - 1 \right| \tag{6.1}$$

$$P_{SG} = \frac{1}{\pi} \cos^{-1} \left(\frac{\sum c_i m_i}{\sqrt{\sum c_i^2 \cdot \sum m_i^2}} \right) \tag{6.2}$$

$$\mathrm{C_{SG}} = 1 - \sqrt{M_{SG}^2 + P_{SG}^2} \tag{6.3}$$

In this context, c and m are two vectors representing generic curves whose correlation is

to be evaluated — in this specific case, the lumbar load measured experimentally and the one obtained from the MADYMO numerical model.

Additional statistics were calculated, offering a further measure of agreement. The percentage error ($E_{\%}$) on the maximum value provides an indication of the difference between the experimental and numerical peak values. The Pearson correlation coefficient (r), on the other hand, measures the degree of correlation between the two curves, evaluating how well the numerical curve reproduces the experimental one. A value equal to 1 indicates a perfect match.

$$\mathrm{E}_{\%} = \left| \frac{\max(c_i) - \max(m_i)}{\max(m_i)} \right| \cdot 100 \tag{6.4}$$

$$r = \frac{n \sum c_i m_i - \sum c_i \sum m_i}{\sqrt{n \sum c_i^2 - \left(\sum c_i\right)^2} \cdot \sqrt{n \sum m_i^2 - \left(\sum m_i\right)^2}} \tag{6.5}$$

6.3.1. Model without Cushion Validation

First, the model was validated in the absence of cushions using the results of the previous experimental campaign to verify the outcomes obtained in [18] with a multibody MADYMO model. This also enables a later comparison between the two configurations, one without and one with the cushion.

Before proceeding with the analysis, it is important to highlight the selection criteria applied to the test data obtained in [18]. Specifically, stiffness values higher than 2270 N/mm were discarded as they exhibited a response similar to that of a fully rigid seat. The configuration with K=104 N/mm was also excluded, as the springs bottomed out, making the experiment no longer meaningful and leading to an excessive increase in lumbar load. Only experimental tests that produced meaningful results were considered. Repeated tests affected by plastic deformation, which led to out-of-scale lumbar load histories, were also disregarded. Furthermore, as anticipated in Table 3.3 and shown in Figure 4.1, in addition to the data from the previous experimental campaign, the verification tests carried out prior to the campaign related to this thesis were also included in the plots, under the label experimental check. Specifically, one test with the fully rigid seat and tests with die springs of stiffness 413 and 709 N/mm were performed, which are comparable with the range used in Thesis [18].

The next pages present the superposed lumbar-load curves along with the resulting validation metrics.

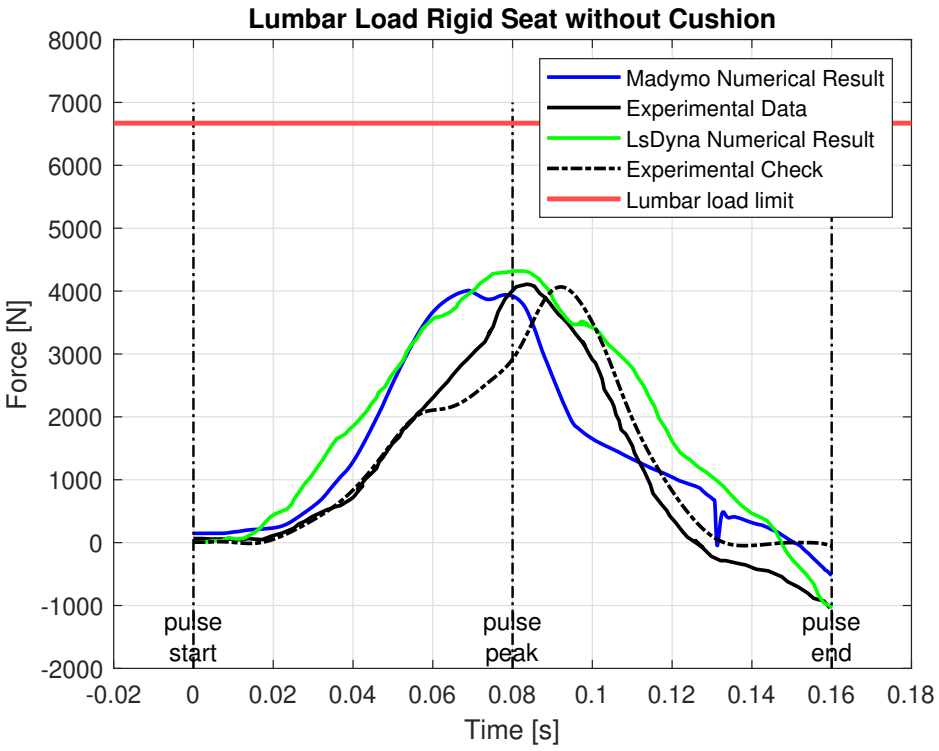

Figure 6.4: Model without Cushion – Rigid Seat

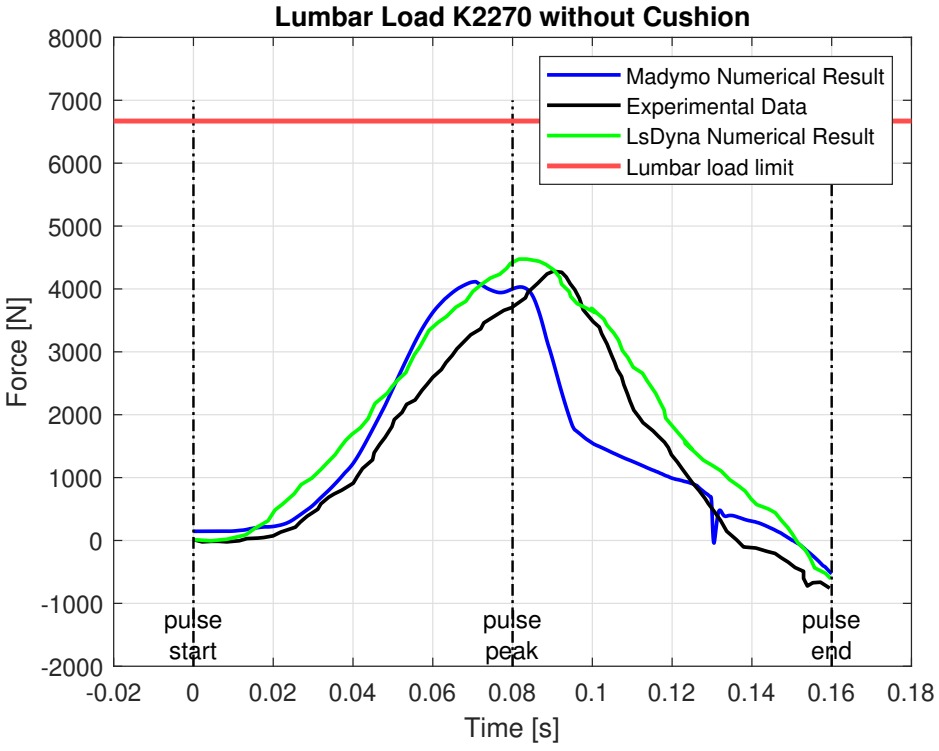

Figure 6.5: Model without Cushion – Seat Stiffness 2270 N/m

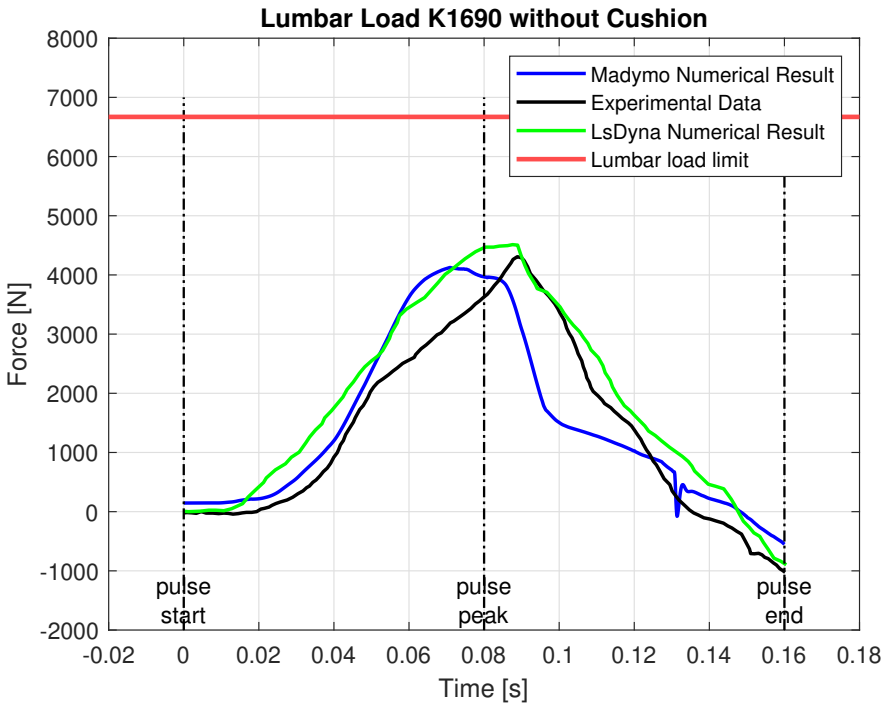

Figure 6.6: Model without Cushion – Seat Stiffness 1690 N/m

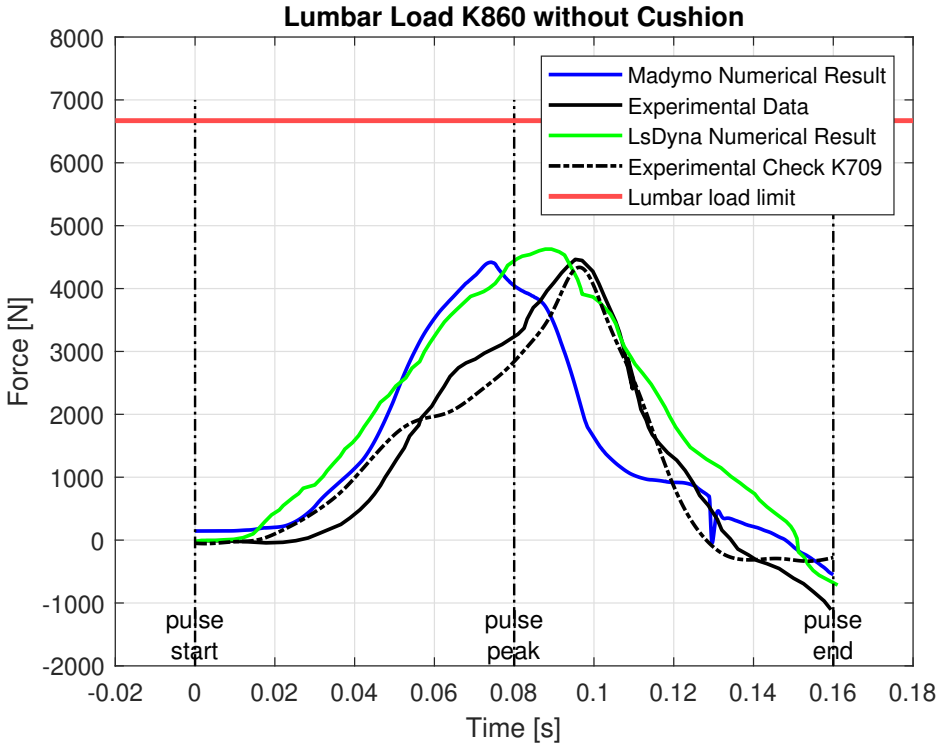

Figure 6.7: Model without Cushion – Seat Stiffness 860 N/m

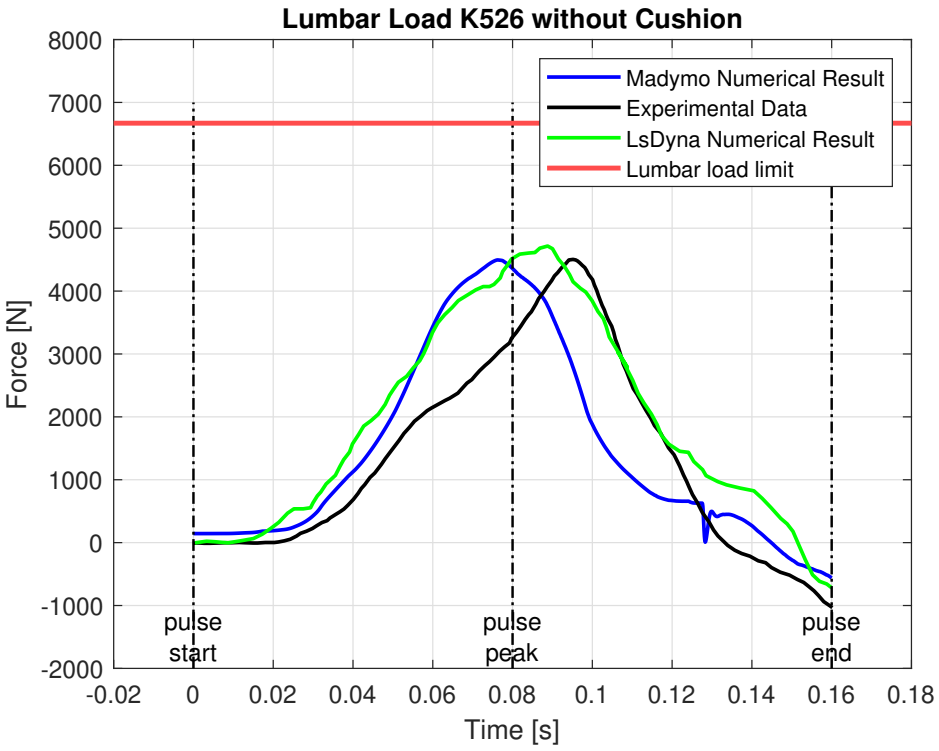

Figure 6.8: Model without Cushion – Seat Stiffness 526 N/m

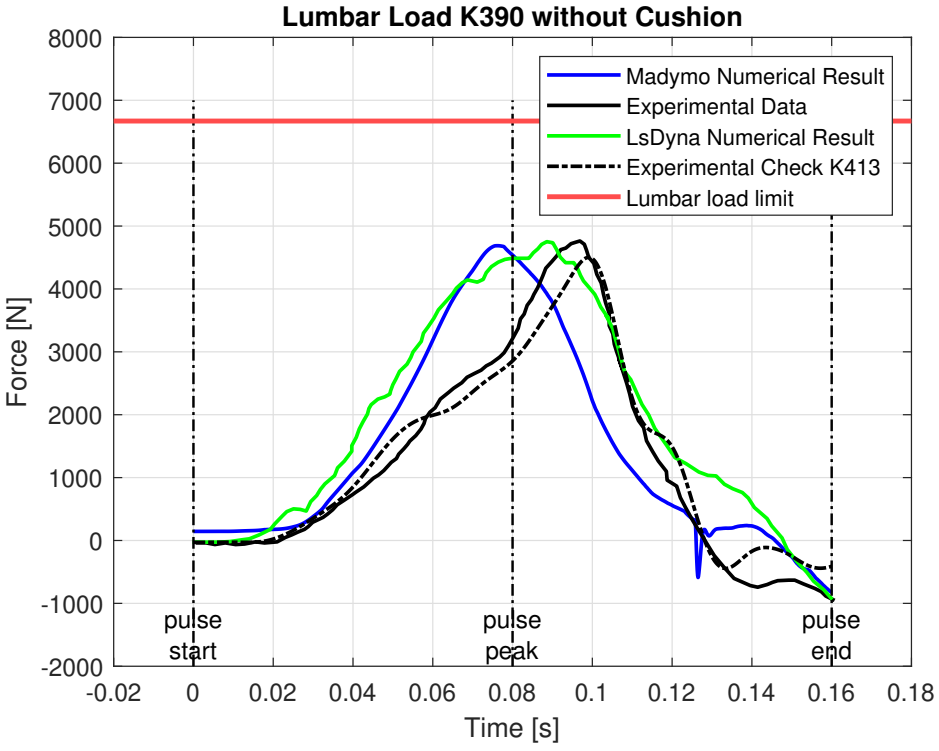

Figure 6.9: Model without Cushion – Seat Stiffness 390 N/m

With this premise, it becomes immediately evident that the MADYMO model accurately reproduces both the shape and the peak of the experimentally obtained lumbar load curve. A few considerations can be made regarding the model: firstly, as with the finite element model, the MADYMO simulation tends to anticipate the lumbar load peak. However, compared to the LS-DYNA model, a better match is observed in terms of the area under the curve, which is more consistent with the experimental data.

Additionally, due to the simplified nature of the multibody model, the lumbar load curve exhibits fewer oscillations than the one obtained with the more complex FEM model.

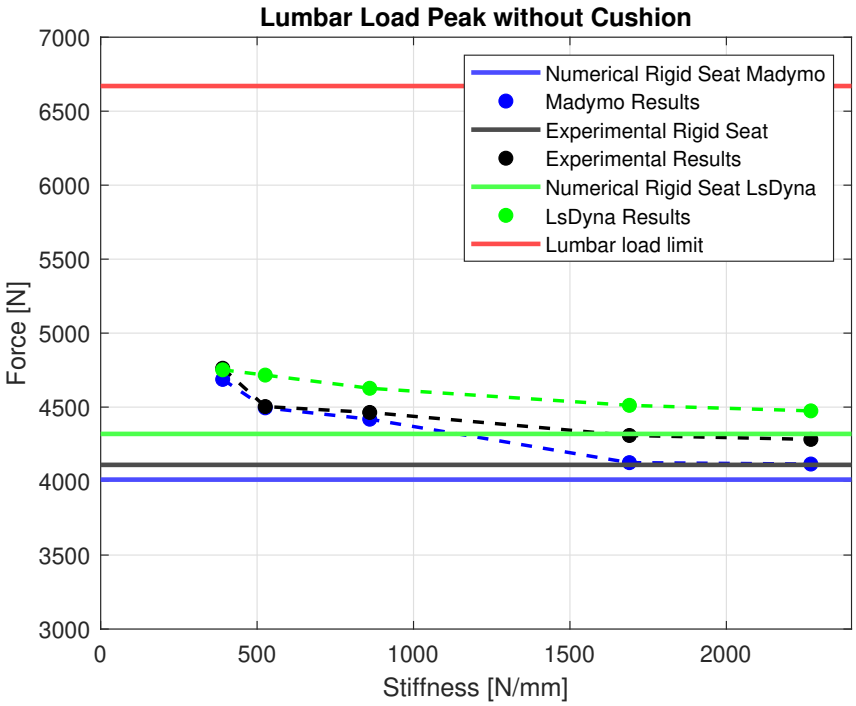

Figure 6.10: Lumbar Load Peak without Cushion

Looking more closely at the lumbar load peaks in Figure 6.10, both models provide a good approximation, although the FEM model tends to overestimate the peak values, while the multibody model slightly underestimates them. In any case, the multibody simulations confirmed the expected behaviour, showing a reduction in lumbar load peak as seat stiffness increases, with minimum values observed for rigid seat configuration.

In addition to the previous qualitative analysis of the curves, the following Table 6.1 presents the results of the quantitative correlation analysis between the experimental and numerical curves, through the calculation of the Sprague and Geers coefficients, the Pearson correlation coefficient, and the percentage error on the lumbar load peak.

Stiffness [N/mm]	**C_{SG}** [-]	**r** [-]	**$E_{\%}$** [%]	**Exp peak** [N]	**Num peak** [N]
Rigid	0.8669	0.8586	2.51	4010	4110
2270	0.8772	0.9298	2.74	4115	4228
1690	0.9095	0.9307	4.46	4124	4308
860	0.8643	0.8814	1.04	4418	4464
526	0.8269	0.8318	0.20	4495	4504
390	0.8177	0.8307	1.60	4687	4762

Table 6.1: Correlation Results without Cushion

It can be observed that the C_{SG} coefficient ranges between 0.8 and 0.9, deviating slightly from the unit value. This indicates a fair overall agreement between the experimental and numerical curves, both in terms of shape and peak magnitude. In more detail, the M_{SG} coefficients, which reflect the accuracy of the peak, are more satisfactory than the P_{SG} coefficients related to the curve shape. The deviation from unity is therefore almost entirely due to differences in the shape of the two curves. Supporting these observations, the Pearson correlation coefficient r, which accounts solely for the similarity in the curve trends, also confirms this correlation. In fact, in the experimental tests several factors may introduce a slight delay in the load curve and thus in the instant at which the peak occurs. The braking system itself, the transmission of the deceleration to the dummy, and the non-ideal dynamics of how the dummy's back moves and transfers load to the lumbar load cell can all influence this behavior.

Nevertheless, it is evident that, despite the earlier response observed in both LS-DYNA and MADYMO models compared to the experimental tests, the area under the numerical and experimental curves, especially in the multibody case, remains consistent. Most importantly, the peak lumbar load value, which represents the fundamental quantity to be compared against the regulatory limit of 6670 N, is accurately captured by the model. The percentage errors on the lumbar load peaks are well below the 10% threshold typically considered acceptable for validation purposes, with the maximum error remaining under 5%. This confirms that the most critical parameter, namely the peak lumbar load, is reliably reproduced by the model, while discrepancies in the curve shape play only a secondary role.

A final check addressed a key feature of this research: the springs. The maximum elongation predicted by the numerical model was compared with that measured in the tests to ensure the spring behaviour was replicated faithfully.

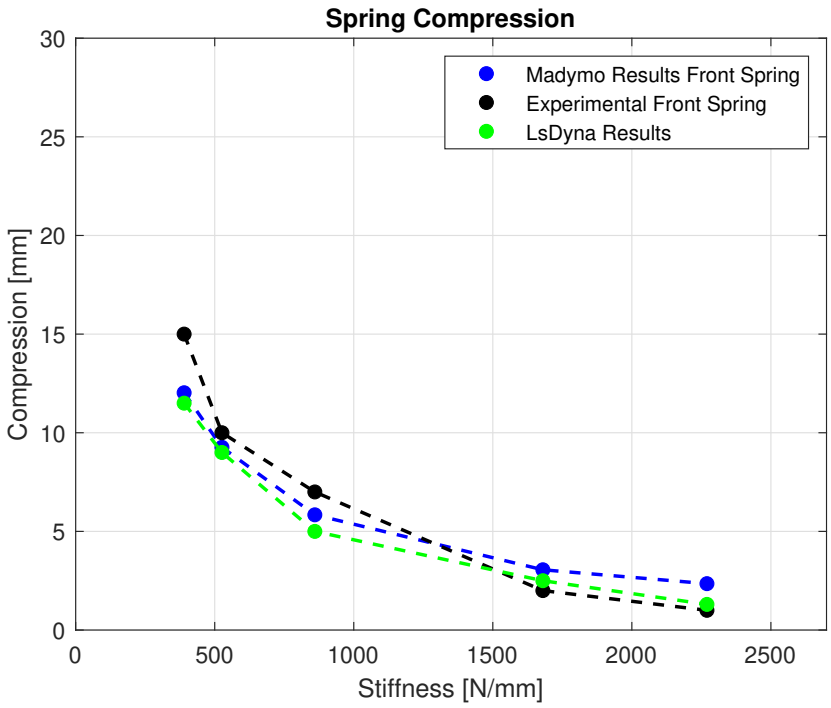

Figure 6.11: Spring Compression without Cushion Validation

The behavior of the springs also matches the experimental observations. A slight underestimation of spring compression is noted for the softer configurations, while a tendency to overestimate is observed for the stiffer ones. However, while spring elongation can be reliably extracted from the numerical model outputs, especially for small deformations, this is not equally true for the experimental data. In fact, for small displacements, the video analysis and image correlation performed using Phantom software, both via automatic tracking of reference points and manual input, show uncertainties comparable to the measured displacements themselves. Therefore, this part of the experimental data cannot be considered fully reliable. Nevertheless, despite this approximation, particularly relevant for the stiffer springs, the overall trend is accurately reproduced, confirming the validity of the model also from this perspective.

6.3.2. Model with Cushion Validation

Secondly, the modified model including the cushion was validated using the experimental data obtained during the test campaign described in the reference.

The following plots show the time histories of the lumbar load predicted by the MADYMO model compared to those measured experimentally.

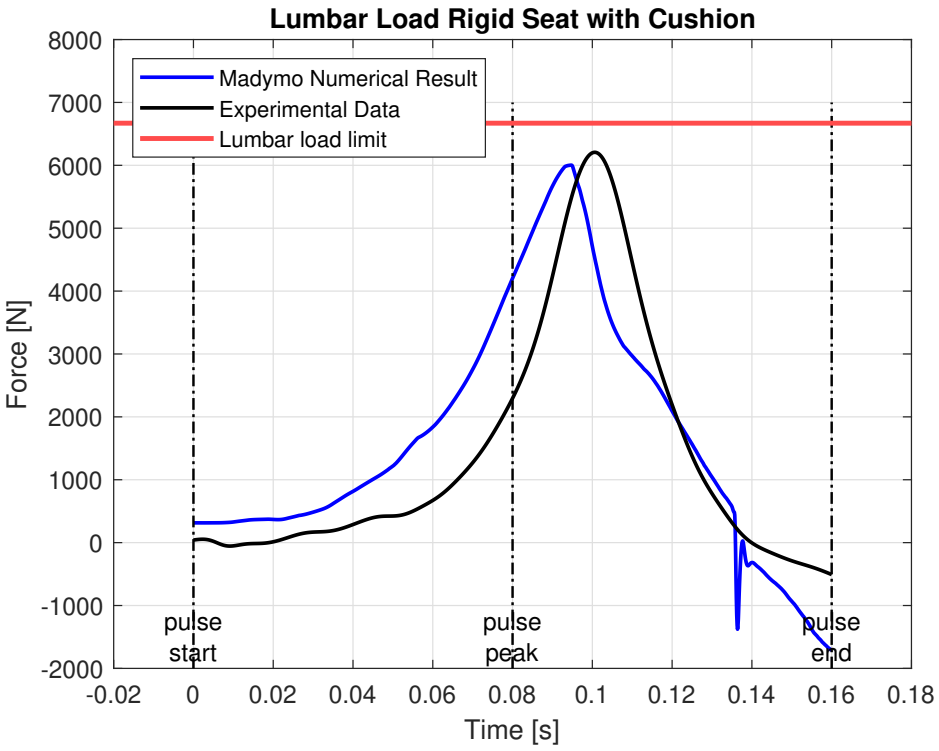

Figure 6.12: Model with Cushion – Rigid Seat

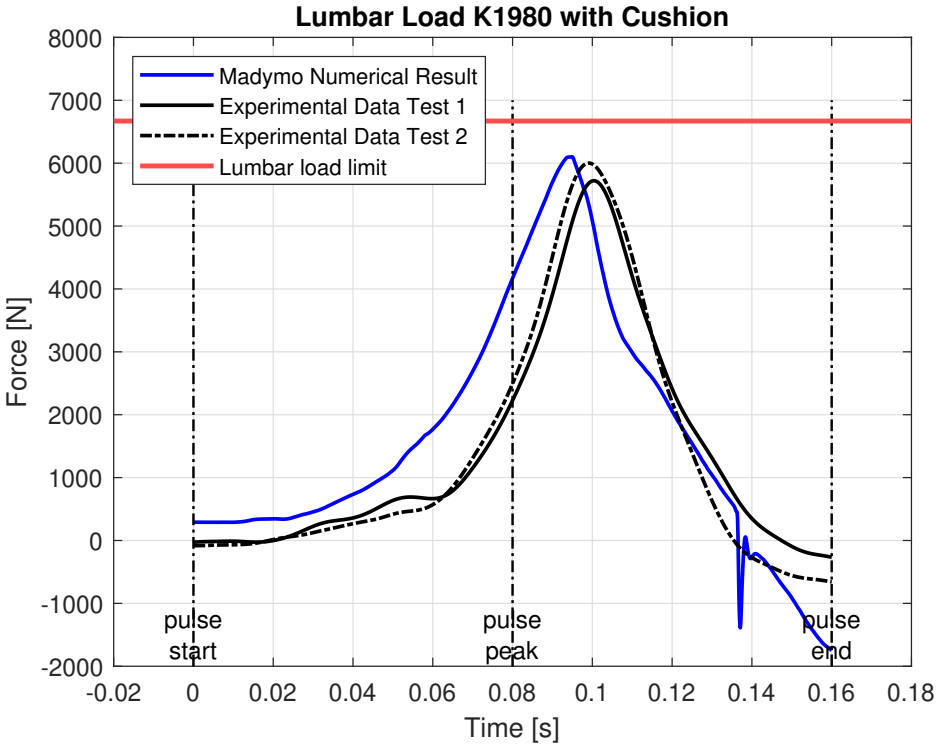

Figure 6.13: Model with Cushion – Seat Stiffness 1980 N/m

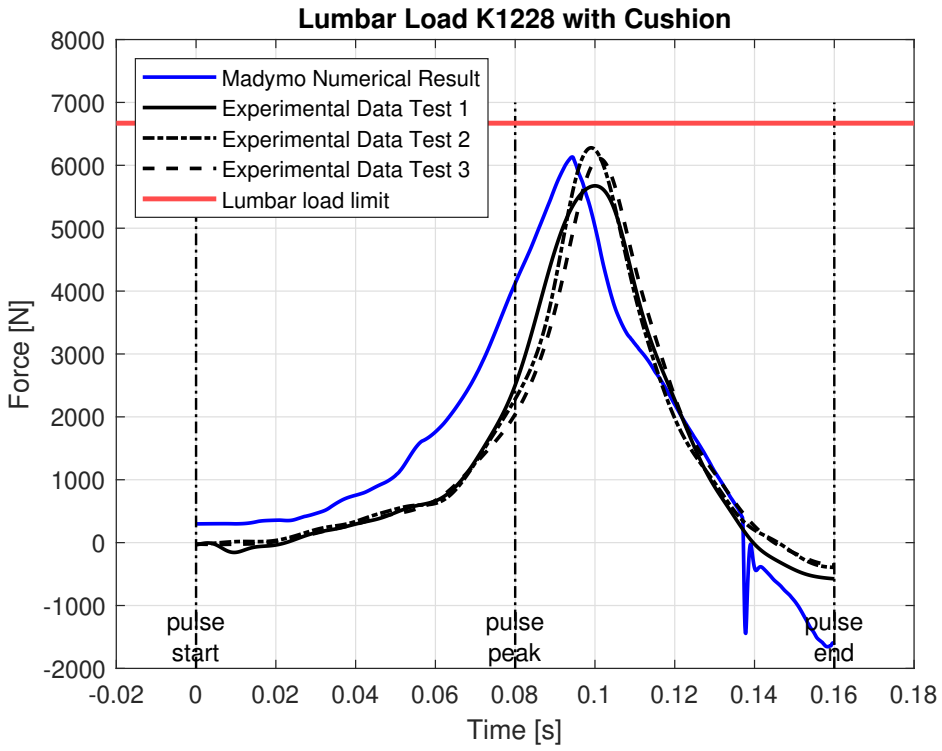

Figure 6.14: Model with Cushion – Seat Stiffness 1228 N/m

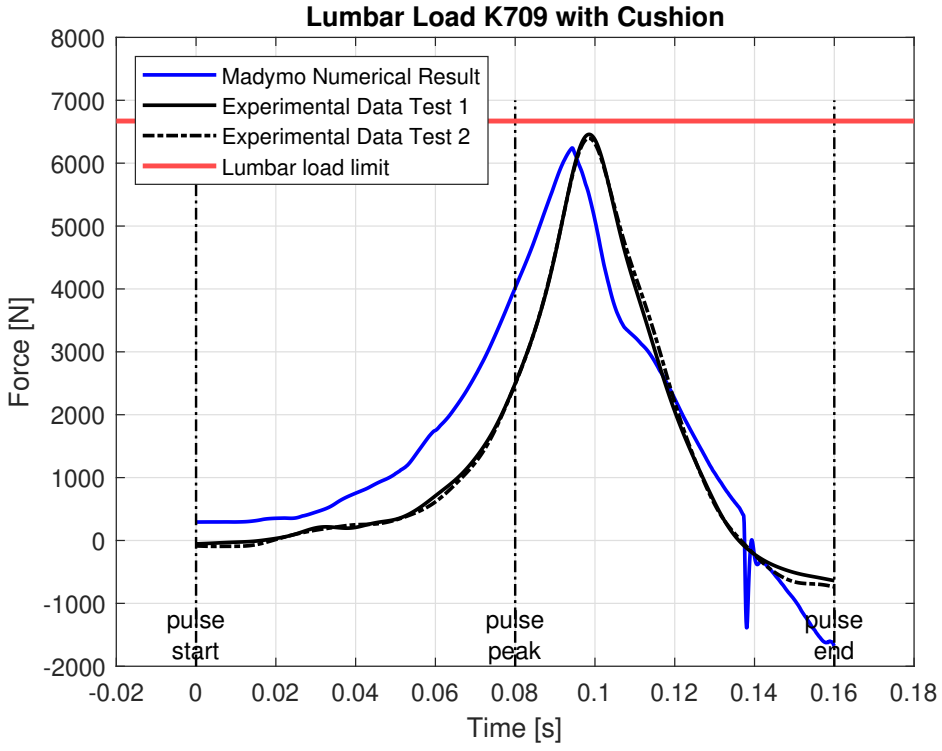

Figure 6.15: Model with Cushion – Seat Stiffness 709 N/m

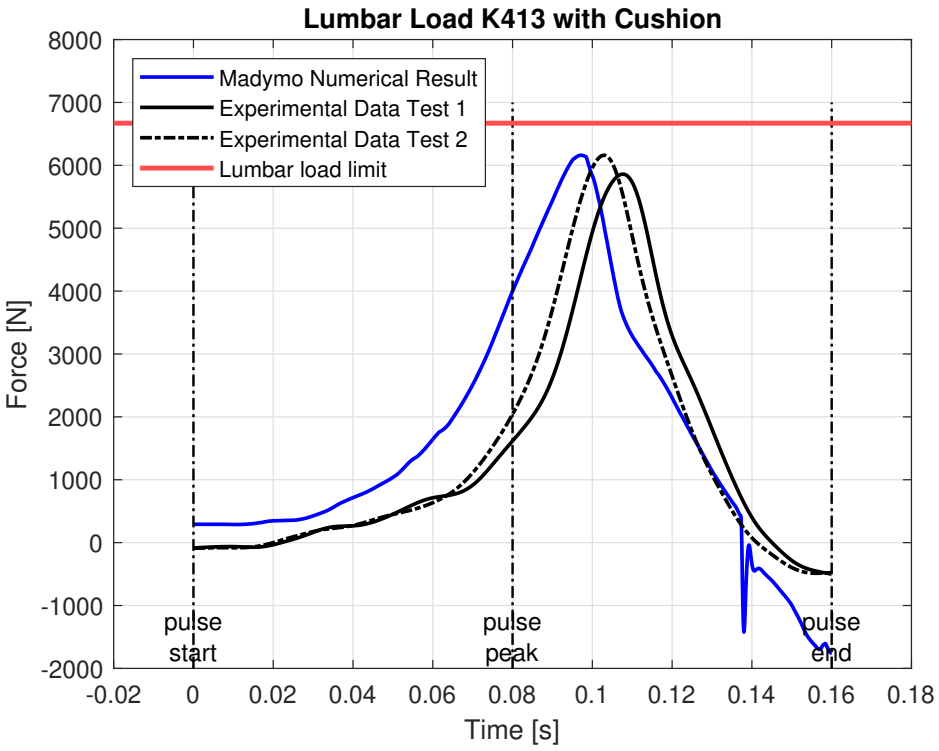

Figure 6.16: Model with Cushion – Seat Stiffness 413 N/m

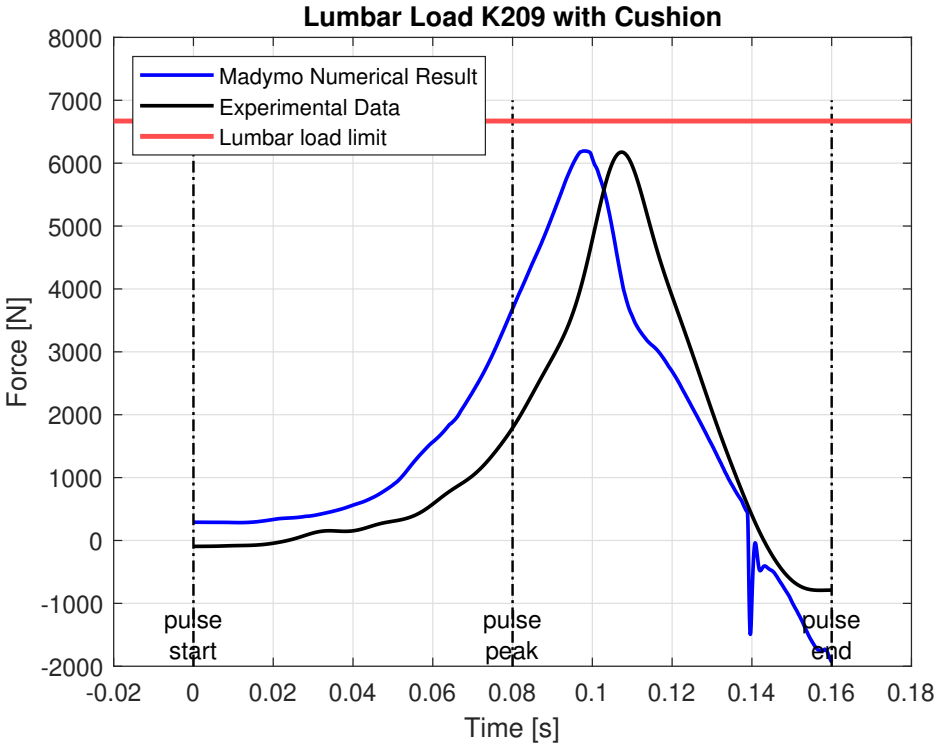

Figure 6.17: Model with Cushion – Seat Stiffness 209 N/m

Also in this case, a good agreement in terms of shape and an accurate reproduction of the lumbar peak load are observed. The main discrepancy remains the anticipation of the peak, although the time shift is reduced compared to the case without the cushion, this time, the anticipation is limited to a few instants. Finally, the unloading phase of the lumbar load cell, corresponding to the moment when the dummy detaches from the seatback, is captured more accurately than the loading phase.

A closer analysis of the lumbar peak loads in Figure 6.18 reveals that, compared to the experimental values, the numerical results show a smaller variation of the peak as a function of seat stiffness. This further supports the previously discussed hypothesis: the presence of the cushion substantially cancels out the influence of the springs, and the numerical model highlights this behavior even more clearly. Moreover, also in this case, no evident increasing or decreasing trend can be identified when seat stiffness and cushion effects act simultaneously.

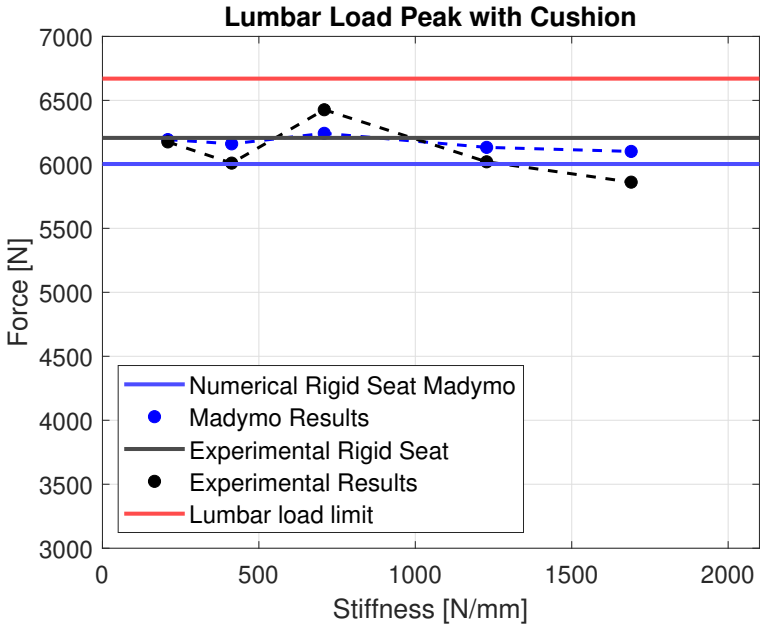

Figure 6.18: Lumbar Load Peak with Cushion

Similar considerations to the model without cushion can be drawn from the analysis of the coefficient values reported in Table 6.2. In particular, the coefficient C_{SG} shows only a limited deviation from unity, indicating good agreement between experimental and numerical curves in terms of both shape and peak. Once again, the main differences can be attributed to the curve shape rather than to the lumbar peak value, with the multibody model showing a tendency to anticipate the experimental tests. Nevertheless, the area under the curves remains consistent, while the maximum value is accurately

reproduced. The Pearson correlation coefficient r further confirms the similarity in trend. Most importantly, the percentage error on the lumbar load peak remains well below the 10% threshold typically accepted for validation purposes, with the maximum error not exceeding 5%. The peak values are around 6100 N, due to the presence of the cushion which, through dynamic interaction with the dummy, increases the lumbar load. Although this brings the load closer to the injury threshold, the values remain safely below the regulatory limit of 6670 N.

Stiffness [N/mm]	$\mathbf{C_{SG}}$ [-]	**r** [-]	$\mathbf{E_{\%}}$ [%]	**Exp peak** [N]	**Num peak** [N]
Rigid	0.8478	0.8655	3.27	6206	6003
1980	0.8621	0.9052	4.09	5861	6101
1228	0.8165	0.8608	1.88	6020	6133
709	0.8692	0.9237	2.86	6426	6242
413	0.8305	0.8864	2.50	6010	6160
209	0.8205	0.8346	0.29	6175	6193

Table 6.2: Correlation Results with Cushion

A final verification focused on one of the key aspects of this study: the springs. The maximum elongation predicted by the numerical model was compared with the experimental measurements to assess the accuracy with which the spring behavior was reproduced.

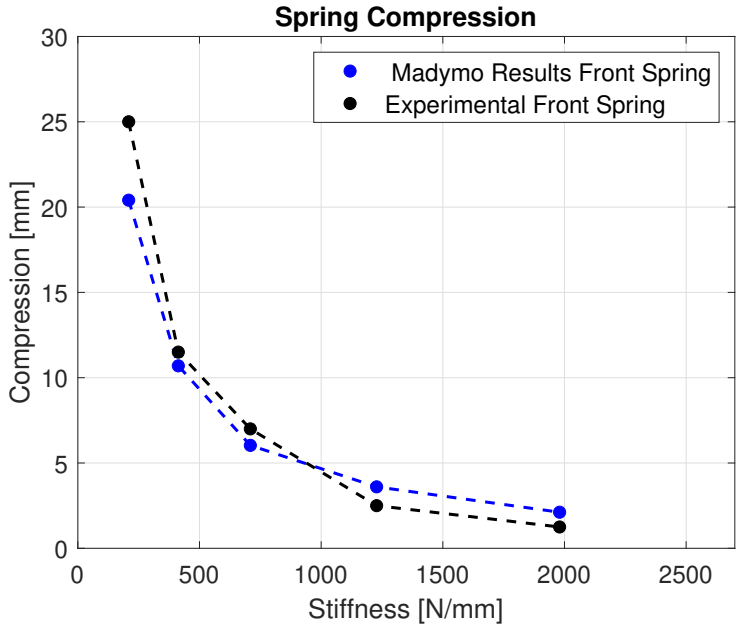

Figure 6.19: Spring Compression without Cushion Validation

The behavior of the springs in Figure 6.19 also matches the experimental observations, as already observed in the configuration without the cushion. A slight underestimation of spring compression is noted for the softer configurations, while a tendency to overestimate is observed for the stiffer ones.

A noteworthy consideration concerns the spring with a stiffness of 209 N/mm. Experimentally, this spring was observed to bottom out approximately at the deceleration peak, while the numerical model predicted a slightly lower compression of about 4 mm, thus failing to fully replicate the observed behavior. This discrepancy is attributed to setup constraints. In the model, the only forces acting on the springs before deceleration were those due to the seat and the dummy's weight. Experimentally, however, it was necessary to preload the springs by tightening them with bolts, which introduced an additional preload and consequently an initial compression.

To minimize asymmetries, a torque wrench was used to tighten the bolts with consistent torque, thereby avoiding uneven precompression across the four springs mounted under the seat. The precompression was then measured with a caliper. For the stiffer springs, no measurable precompression was found, while the intermediate ones showed displacements of approximately 1 mm. The softer springs were subjected to greater precompression. Specifically, the 209 N/mm spring, which was already expected to approach full compression, showed a 4 mm precompression due to the tightening process. This explains the discrepancy between numerical and experimental behavior.

Nevertheless, for the stiffer springs, which were far from bottoming out, precompression played only a marginal role. As explained earlier, an additional source of uncertainty in estimating the compression of the stiffer springs during the experimental tests arises from the video analysis itself: when dealing with very small displacements, the measurement becomes highly imprecise, with uncertainties comparable to the displacement being measured. Therefore, the imperfect correspondence in the spring behavior should be attributed primarily to this effect rather than to a deficiency of the model. Moreover, since the cushion dynamically decouples the dummy from the springs, this small mismatch in spring behavior did not compromise the accuracy of the lumbar load prediction.

6.3.3. Results Comparison

After validating the models, it becomes of interest to compare the differences under the same ideal deceleration profile between the effect of seat stiffness alone and the combined effect of cushion and springs. This comparison aims to highlight how the dynamic coupling introduced by the additional components influences the resulting lumbar load.

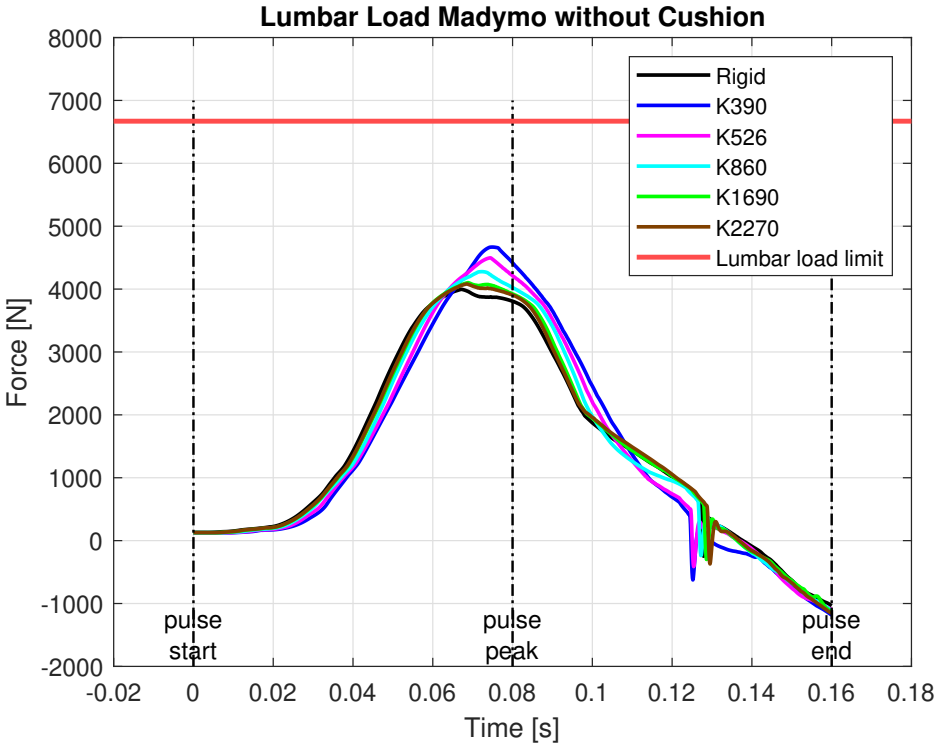

(a) Ideal Deceleration without Cushion

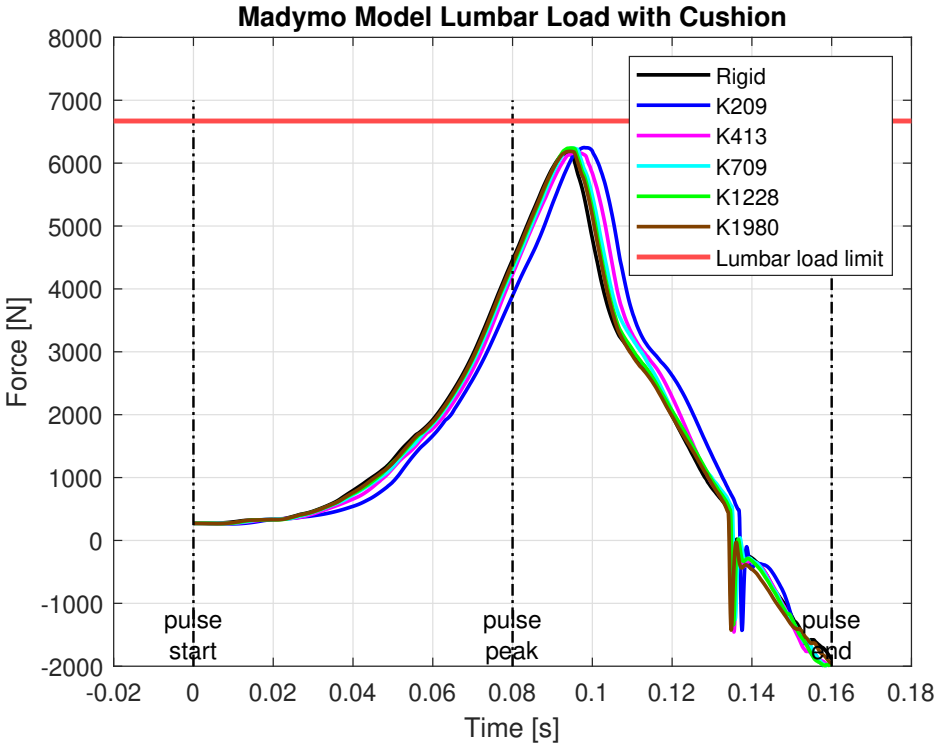

(b) Ideal Deceleration with Cushion

Figure 6.20: Models Comparison

In Figure 6.20 it is observed that, in the absence of a cushion, the difference in peak lumbar load between the fully rigid seat and the softest spring configuration is approximately 650 N. This indicates that a less stiff seat significantly increases the lumbar load. When the cushion is included in the model, the peak load increases as expected, but the variation between different stiffness values becomes smaller and does not exhibit a clear trend. The maximum variation in peak lumbar load, at equal model conditions and only varying the seat stiffness, is around 95 N. This result shows that the influence of seat stiffness is strongly reduced when a polyurethane foam cushion is present, due to the altered dynamics during deceleration.

7 | Scaling to a Real Aircraft Seat

The seat used in the dynamic tests and subsequently replicated in the numerical model does not reflect the characteristics of actual aeronautical seats. Specifically, to ensure complete rigidity, the upper part of the seat used for testing weighs 50 kg, which is far heavier than what would be acceptable for real aircraft seating. Weight reduction is a critical design factor in aeronautical seats, and the mass of this component in a typical aircraft seat is around 10 kg. Since the goal of this thesis is to evaluate the impact of seat stiffness on the lumbar spine load experienced by passengers in real-world conditions, the numerical model, initially validated with the 50 kg seat, was adapted and scaled to reflect a more realistic 10 kg seat configuration.

To achieve this, new mass properties were assigned to the seat in the model. This required recalibrating the spring stiffness to maintain consistent performance. Specifically, the relationship between the kinetic energy of the seat and dummy, and the elastic potential energy of the spring at maximum deflection, was preserved, ensuring the proper operation of the spring. The kinetic energy of the moving part of the setup was calculated for both the 50 kg and 10 kg seat configurations by estimating the masses and integrating the velocity from the prescribed acceleration defined by the regulation. The potential energy at the point of maximum spring compression was then determined for the 50 kg configuration and, through proportionality, the corresponding potential energy for the lightweight aircraft seat was obtained. From this potential energy, the maximum compression, assumed equal to that observed in the tests with the heavier seat, was imposed, enabling the estimation of the scaled stiffness value for the springs of the 10 kg seat.

For the 10 kg scaled seat, the stiffness range was reduced from the original 209–1980 N/mm to 142–1341 N/mm. Specifically, the correspondence between the spring stiffness and the equivalent global seat stiffness is as follows:

- 209 N/mm spring stiffness corresponds to 142 N/mm
- 413 N/mm spring stiffness corresponds to 280 N/mm

- 709 N/mm spring stiffness corresponds to 480 N/mm
- 1228 N/mm spring stiffness corresponds to 832 N/mm
- 1980 N/mm spring stiffness corresponds to 1341 N/mm

These spring stiffness values were subsequently implemented in the 10 kg seat model, and simulations were performed to verify the behavior and assess the results.First, the behavior of the springs representing the different seat stiffness values was analyzed in order to verify their proper correspondence.

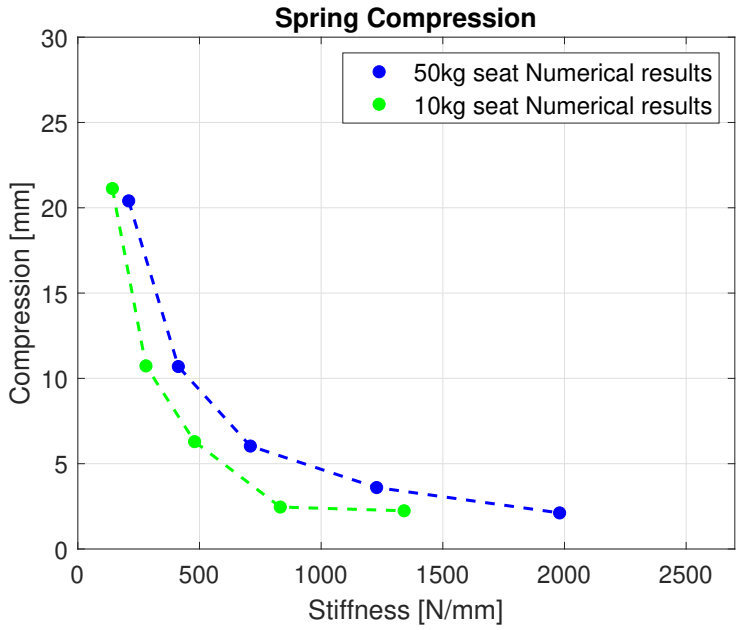

Figure 7.1: Spring Compressions Validation

As shown in Figure 7.1, the maximum deflection of the newly calibrated springs aligns closely with that of the springs used in the original 50 kg seat simulation. For example, in the 10 kg seat model, when a spring with a stiffness of 142 N/mm is used, it compresses by 20 mm, a value consistent with the 21 mm compression recorded for the 209 N/mm springs in the 50 kg seat configuration. Conversely, the spring with a stiffness of 1342 N/mm compresses by only 2 mm in 10 kg seat model, behaving almost as a rigid component, as expected from the 1980 N/mm case in 50 kg model, where the compression was also 2 mm. For the other stiffness values as well, the correspondence in the spring compression is excellent.

The lumbar load responses of both models subjected to the ideal deceleration pulse are presented below.

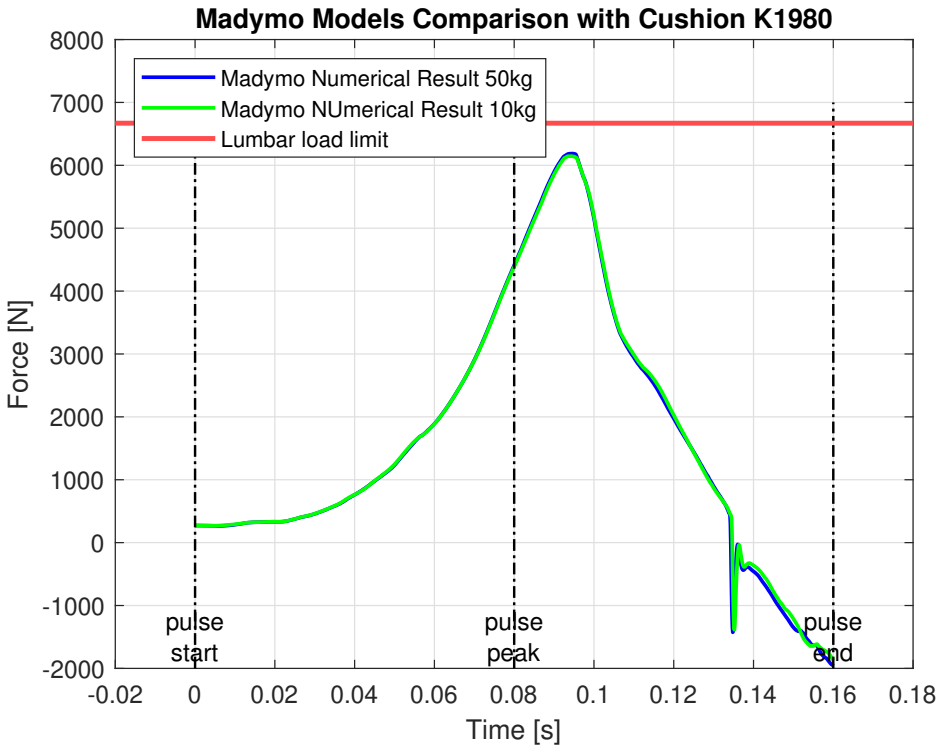

Figure 7.2: Models Comparison – K = 1980 N/mm & K = 1342 N/mm

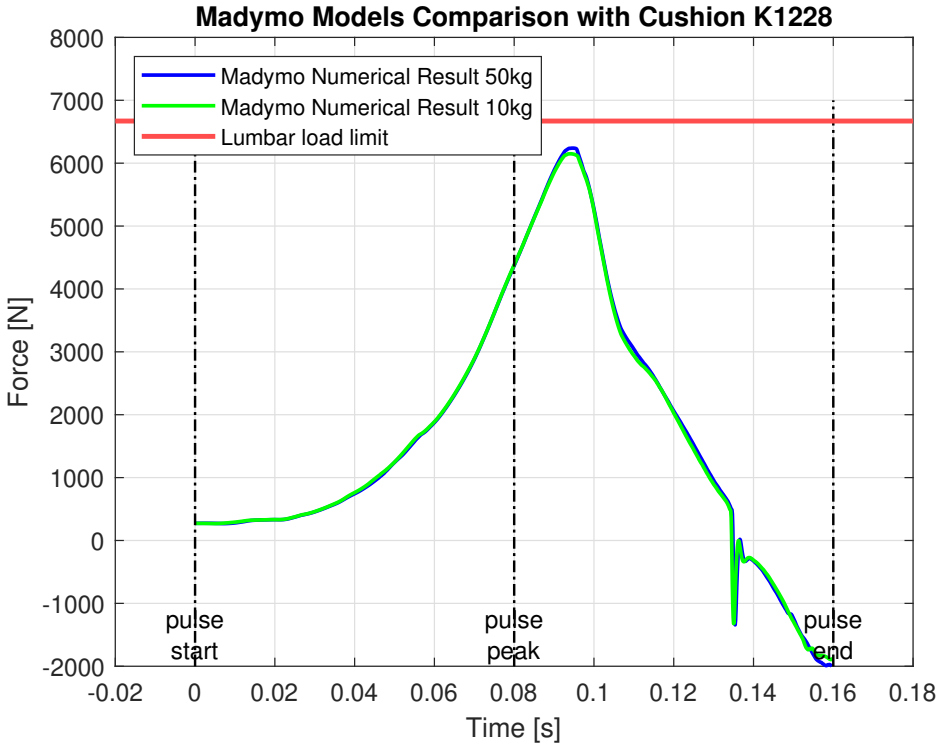

Figure 7.3: Models Comparison – K = 1228 N/mm & K = 832 N/mm

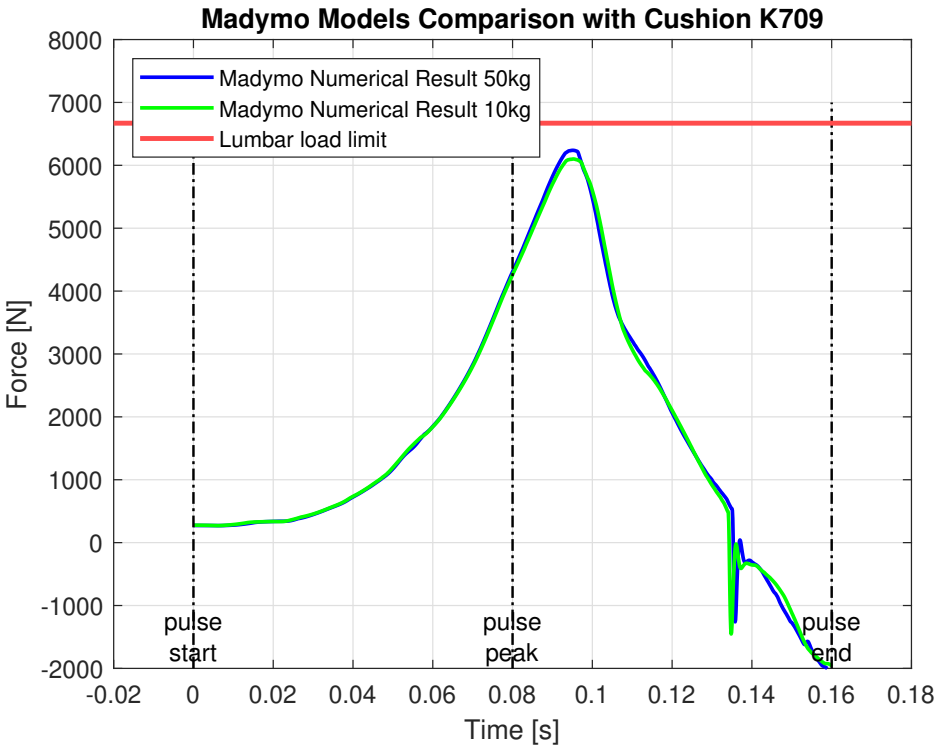

Figure 7.4: Models Comparison – K = 709 N/mm & K = 480 N/mm

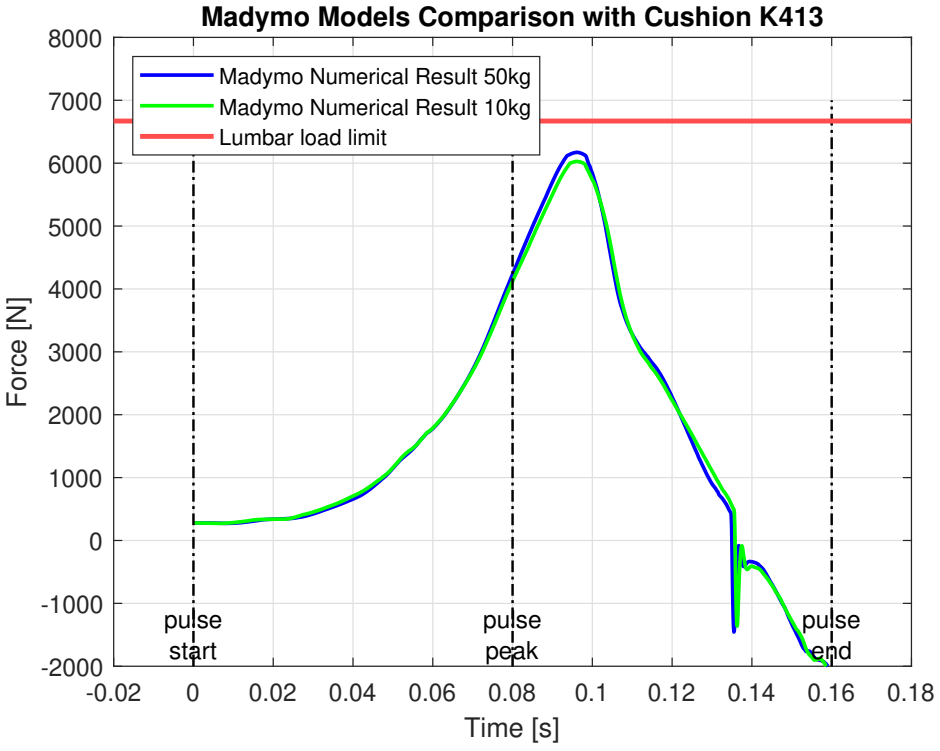

Figure 7.5: Models Comparison – K = 413 N/mm & K = 280 N/mm

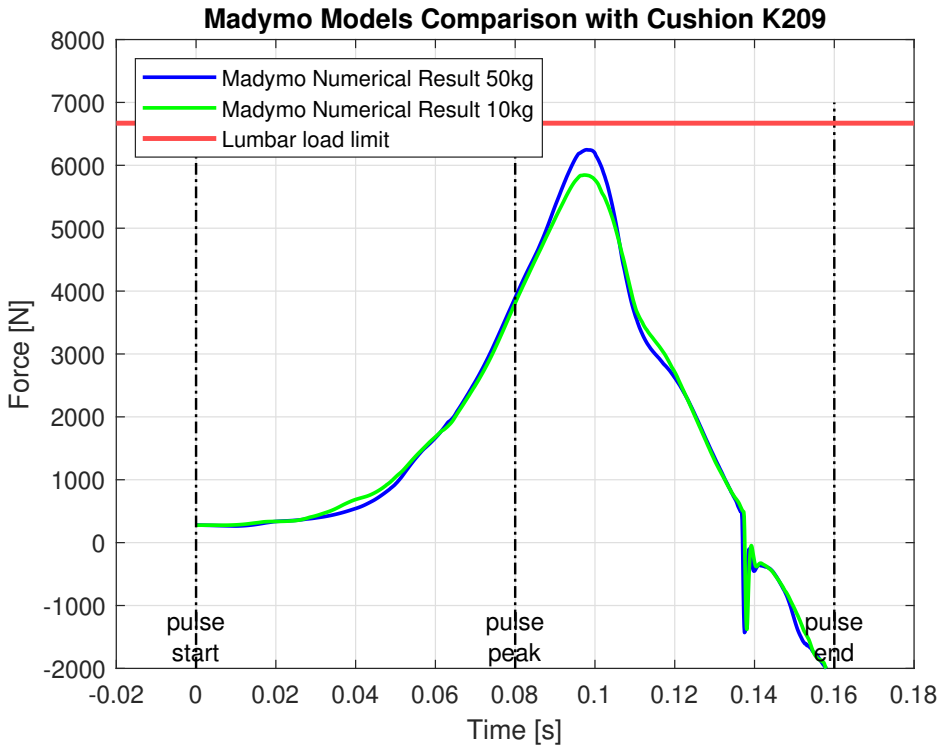

Figure 7.6: Models Comparison – K = 209 N/mm & K = 142 N/mm

It is immediately evident that the overall shape of the curves remains similar; however, a variation in the lumbar load peak values can be observed, as shown in Figure 7.7.

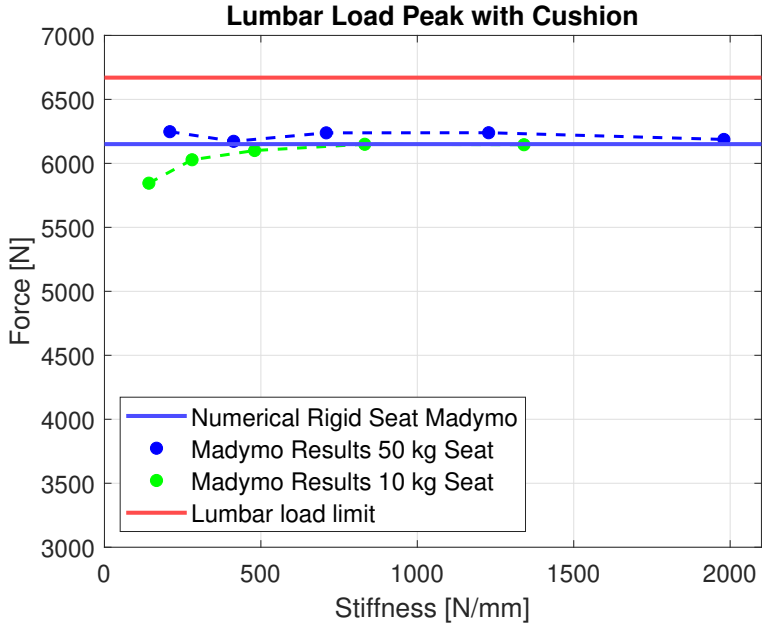

Figure 7.7: Models Comparison – Lumbar Load Peak

A nearly perfect agreement is observed when the spring stiffness is high. In particular, for the 10 kg seat configuration, the response aligns even more closely with the reference case of a completely rigid seat, compared to the 50 kg seat. However, an important trend emerges as the stiffness decreases: a reduction in the lumbar load peak is observed. Specifically, in the presence of the cushion and with a 10 kg aeronautical seat, the lumbar load appears to decrease with decreasing seat stiffness. This behavior is opposite to what is observed in the absence of the cushion, where the lumbar load increases as the stiffness decreases.

This phenomenon can be attributed to the altered dynamics introduced by the lighter seat. Indeed, a lighter seat is likely to induce a smaller initial compression in the springs compared to a 50 kg seat. As a result, the lower amount of energy transferred by the seat to the springs leads to a reduced decoupling between the cushion and the seat stiffness. The dummy gradually compresses the cushion up to a maximum value, while the springs are slightly preloaded by the seat alone. Maximum spring compression is then reached only once the dummy has fully compressed the cushion and transmits additional energy to the seat structure.

This dynamic suggests that a seat with lower stiffness, in combination with the cushion, may contribute to reducing the lumbar load. The MADYMO model shows that with a spring stiffness of 142 N/mm and a 10 kg seat, the lumbar load peak decreases by approximately 300 N compared to the rigid configuration, which represents a non-negligible reduction.

Two further considerations must be addressed. First, it remains essential to explore stiffness values that are compatible with real, manufacturable structures. Secondly, the bottom-out condition must be considered. While the 142 N/mm spring behaves linearly and does not reach the maximum compression limit, lower stiffness values, although potentially beneficial in further reducing lumbar load, must be carefully assessed. They may lead to excessive compression, bottoming out, and thereby deviating from the desired linear behavior, possibly increasing lumbar load again.

Finally, it is worth noting that the 10 kg seat configuration has not yet been validated against experimental data. Therefore, conducting a dedicated test campaign with a real aeronautical seat would be valuable to confirm these findings.

8 | Conclusions and Future Developments

The intent of this study was to investigate the influence of seat stiffness, when combined with a cushion, on the maximum lumbar spine load. To this aim, the stiffness of the seat was modeled through four springs placed at the corners of the seat base, and a polyurethane foam cushion was positioned under the pelvis of the dummy.

A test campaign was carried out in which several deceleration tests were performed, with reference to the *CS 25* regulation.

A multibody model was developed using MADYMO software. First, the model was validated in the absence of the cushion to confirm previous findings [18]. As with the finite element model, the multibody model confirmed the experimental results: without the cushion, the lumbar peak load increases as the seat stiffness decreases.

Subsequently, the cushion was added to the model. Once again, the model results were consistent with the experimental data and revealed a different behavior. In the presence of springs and a cushion, a dynamic decoupling occurs. The dummy is decelerated by the cushion while the springs are initially compressed by the seat alone. When the cushion reaches its maximum compression, the springs have already reached their maximum deflection. This means that the seat stiffness acts immediately during deceleration, but the dummy is still compressing the cushion. As a result, the dummy applies its load to a seat that is already fully compressed. In practice, the seat behaves as a rigid component once the dummy reaches the end of its displacement. Therefore, the effect of seat stiffness is obscured, and only the effect of the cushion is visible.

All the results obtained from the model and experimental tests, regardless of the seat stiffness value, produced lumbar loads of approximately 6100 N, which corresponds to the value measured in the configuration with a completely rigid seat and cushion only.

Since the numerical model has been validated, minor modifications can be introduced to expand the range of investigated conditions. One such case was the insertion of a realistic

seat mass. In this scenario, the numerical model revealed an even more complex dynamic. The seat does not possess sufficient energy to fully preload the springs on its own while the dummy compresses the cushion. Therefore, when the dummy compresses the cushion and then transfers its energy to the seat, the springs are still actively deforming. This behavior, in which the cushion first slows down the dummy and then transfers the force to the springs, leads to a trend where the lumbar peak decreases as seat stiffness decreases in the presence of the cushion.

From this work, a conclusion and an opportunity for further research can be drawn. Firstly, it is evident that whenever a polyurethane cushion is added to the seat, it overshadows the effect of seat stiffness. No critical behavior is observed where reduced stiffness leads to an increased lumbar peak. Thus, within the limits of structural integrity, regulatory compliance, wear, and anchorage, the seat structure plays a secondary role compared to the cushion type. Furthermore, it appears that a less stiff seat may actually help reduce the lumbar peak induced by the cushion.

Further research in this area could be of great interest as it may help mitigate the inevitable increase in lumbar load caused by the use of cushions. Therefore, for a given cushion, a seat designed with appropriately reduced stiffness, using engineering solutions such as materials, springs within bottom-out limits, and optimized connections, could effectively couple with the cushion and reduce the increase in lumbar load.

The next logical step for this research would be to carry out a new experimental campaign to validate and confirm the results using a real aircraft seat. Additionally, testing different cushion types could be of great interest. In this work, a soft polyurethane foam cushion was used, but more rigid or high-performance cushions could be considered, including polyurethane foams with higher density or strain-rate sensitive foam solutions such as CONFOR. The different cushion properties could significantly alter the overall response dynamics of the seat-dummy system.

Furthermore, future work could expand the investigation of the cushion by examining the influence of environmental factors such as temperature and humidity on its behavior, as suggested in [31]. Repeated-use hysteresis should also be assessed because it may alter cushion performance and, consequently, lumbar-load measurements across successive tests.

Further developments could combine the cushion with additional seat components to clarify their joint influence on lumbar-spine load. A comprehensive parametric study of all major elements would provide guidance for improving seat crashworthiness and further reducing the risk of severe injury in a crash landing.

Finally, as passenger comfort becomes increasingly important, especially on long-range commercial aviation flights, future research could optimize comfort parameters as proposed in reference [32]. However, this further study must not compromise safety; the goal remains to strike the best balance between seating comfort and an acceptable level of lumbar load protection.

Bibliography

[1] Department for Transport, UK Government. Transport statistics great britain: Passenger casualty rates by mode. `https://www.gov.uk/government/collections/transport-statistics-great-britain`, 19 Dec 2024. Based on data from 2006 to 2023.

[2] Airbus. A statistical analysis of commercial aviation accidents 1958 - 2024. Technical report, Airbus, 2024.

[3] Industry ARC. Global aircraft seat material market (2013–2022), 2022. Market research report.

[4] European Aviation Safety Agency (EASA). *Certification Specifications and Acceptable Means of Compliance for Large Aeroplanes CS-25*. EASA, 5 November 2018. Amendament 22, page 1-C-25, paragraphs CS 25.561 and CS 25.562.

[5] Federal Aviation Administration. Advisory circular ac 25.562-1b: Dynamic evaluation of seat restraint systems and occupant protection on transport airplanes. Technical Report AC 25.562-1B, U.S. Department of Transportation, Federal Aviation Administration, Washington, D.C., January 2006.

[6] Todd R.Hurley and Jill M. Vandenburg. *Small Airplane Crashworthiness Design Guide*. Simula Technologies, Inc., 10016 South 51st Street, Phoenix, AZ 85044, 2002. prepared for AGATE.

[7] J. W. Coltman, C. Van Ingen, N.B. Johnson, and R.E. Zimmnermann. *Aircraft Crash Survival Design Guide. Volume II: Aircraft Design Crash Impact Conditions and Human Tolerance*. Simula Inc., Phoenix, Arizona, 1989. Prepared for the U.S. Army Aviation Research and Technology Activity (AVSCOM), Aviation Applied Technology Directorate, Fort Eustis, VA.

[8] Richard E. Zimmermann and Norman A. Merritt. *Aircraft Crash Survival Design Guide. Volume I: Design Criteria and Checklists*. Simula Inc., Phoenix, Arizona, 1989. Prepared for the U.S. Army Aviation Research and Technology Activity (AVSCOM), Aviation Applied Technology Directorate, Fort Eustis, VA.

[9] Richard E. Zimmnermann, James C. Warrick., Alan D. Lane, Norman A. Merritt, and Akif 0. Bolukbasi. *Aircraft Crash Survival Design Guide. Volume III: Aircraft Structural Crash Resistance.* Simula Inc., Phoenix, Arizona, 1989. Prepared for the U.S. Army Aviation Research and Technology Activity (AVSCOM), Aviation Applied Technology Directorate, Fort Eustis, VA.

[10] S.P. Desjardins, Richard E. Zimmeermann, Akif 0. Bolukbasi, and Norman A. Merritt. *Aircraft Crash Survival Design Guide. Volume IV: Aircraft Seats, Restraints, Litters, and Cockpit/Cabin Delethalization.* Simula Inc., Phoenix, Arizona, 1989. Prepared for the U.S. Army Aviation Research and Technology Activity (AVSCOM), Aviation Applied Technology Directorate, Fort Eustis, VA.

[11] C. Spada. Study of the response of helicopter seat energy absorbers. Master's thesis, Politecnico di Milano, 2016. Supervised by Prof. P. Astori.

[12] P. Astori and F. Impari. Crash response optimisation of helicopter seat and subfloor. *International Journal of Crashworthiness*, Department of Aerospace Science and Technology , Politecnico di Milano, Milano, Italy, 2013.

[13] S.J. Hooper and M.J. Henderson. Development and validation of an aircraft seat cushion component test – vol i. Technical Report DOT/FAA/CT-85/11, United States Department of Transportation, Federal Aviation Administration, Washington, DC, 2005.

[14] P. Astori. Simplified analysis for the estimation of seat cushion response – rev. 8. *Synthesis of results*, Department of Aerospace Science and Technology , Politecnico di Milano, Milano, Italy, 2019.

[15] M. Zanella. Development of a new testing methodology for civil aircraft seat cushion certification. Master's thesis, Politecnico di Milano, 2018. Supervised by Prof. P. Astori.

[16] R. Autenrieth, Herrington, R., and K. Hock. *Flexible Polyurethane Foams.* Midland, U.S.A., 1997.

[17] H. K. Beheshti and H. M. Lankarani. A simplified test methodology for crashworthiness evaluation of aircraft seat cushions. *International Journal of Crashworthiness*, 11(1):27–35, 2006.

[18] G. Martinoli. Influence of the seat stiffness on the lumbar spine load in crash landing conditions. Master's thesis, Politecnico di Milano, 2020. Supervised by Prof. P. Astori.

[19] Society of Automotive Engineers. Performance standard for seats in civil rotorcraft, transport aircraft, and general aviation aircraft. Technical Report AS8049-Rev. B, SAE Aerospace, January 2005.

[20] Jeffrey H. Marcus. Dummy and injury criteria for aircaft crashworthiness. Technical Report DOT/FAA/AM-96/11, Civil Aeromedical Institute Federal Aviation Administration, Oklahoma City, 1996.

[21] Ing. Angelo Dovelli. Il calcolo delle molle ad elica cilindrica in filo a sezione rettangolare o quadra. ANCCEM.

[22] Richard L. DeWeese, David M. Moorcroft, and Amanda M. Taylor. Lumbar load variability in dynamic testing of transport category aircraft seat cushions. Technical Report DOT/FAA/21/09, Civil Aerospace Medical Institute, Federal Aviation Administration, March 2021.

[23] F. di Napoli, A. De Luca, F. Caputo, F. Marulo, M. Guida, and B. Vitolo. Mixed fe–mb methodology for the evaluation of passive safety performances of aeronautical seats. *International Journal of Crashworthiness*, Department of Industrial Engineering, University of Naples "Federico II", Napoli, Italy:314–325, 2018.

[24] Siemens Digital Industries Software. *Theory manual, Version 2206.* Simcenter Madymo, 2022.

[25] Siemens Digital Industries Software. *Reference manual, Version 2206.* Simcenter Madymo, 2022.

[26] Siemens Digital Industries Software. *Model manual, Version 2206.* Simcenter Madymo, 2022.

[27] Marta Carvalho Jorge A.C. Ambrósio. Identification of optimal multibody vehicle models for crash analysis. *Journal of Theoretical and Applied Mechanics*, IDMEC – IST, Technical University of Lisbon Av. Rovisco Pais 1, 1049-001 Lisboa, Portugal, 2010.

[28] Nilesh Dhole, Vikas Yadav, and Gerardo Olivares. Certification by analysis of a typical aircraft seat. *12th International LS-DYNA Users Conference*, Computational Mechanics, National Institute for Aviation Research, Wichita; KS 67260; USA, 2012.

[29] Staff of Anthropology Research Project. Anthropometric source book. Technical Report Volume I: Anthropometry for Designers, NASA National Aeronautics and Space Administration, July 1978.

[30] Mario Mongiardini, Chuck Plaxico, and Malcolm Howard Ray. Development of a programme for the quantitative comparison of a pair of curves. *International Journal of Computer Applications in Technology*, Vol. 46, No. 2, 2013.

[31] A. Opreni, S. Mariani, M. Dossi, and M. Brennan. Combined effects of temperature and humidity on the mechanical properties of polyurethane foams. *Journal of Rheology*, Vol. 64, 161–176:Dipartimento di Ingegneria Civile e Ambientale, Politecnico di Milano, Piazza Leonardo da Vinci 32, 20133 Milano, Italy, 2020.

[32] Amalia Vanacore, Antonio Lanzotti, Chiara Percuoco, Agostino Capasso, and Bonaventura Vitolo. Design and analysis of comparative experiments to assess the (dis-)comfort of aircraft seating. *Applied Ergonomics*, Dept. of Industrial Engineering, University of Naples Federico II, 80125, Naples, Italy:155–263, 2019.

List of Figures

List of Tables